Distinct roles for precession, obliquity and eccentricity in Pleistocene 100kyr glacial cycles*

Stephen Barker[1**], Lorraine E. Lisiecki[2], Gregor Knorr[1,3], Sophie Nuber[1***], Polychronis C. Tzedakis[4]

1. School of Earth and Environmental Sciences, Cardiff University, UK
2. Department of Earth Science, University of California, Santa Barbara, USA
3. Alfred Wegener Institute for Polar Research, Bremerhaven, Germany
4. Environmental Change Research Centre, Department of Geography, University College London, UK

** Corresponding author barkers3@cf.ac.uk
*** Now at Department of Oceanography, University of Washington, USA

The final version of this manuscript will be available via
doi: 10.1126/science.adp3491

Submitted Manuscript: Confidential
Template revised July 2024

Title: Distinct roles for precession, obliquity and eccentricity in Pleistocene 100kyr glacial cycles

Authors: Stephen Barker[1]*, Lorraine E. Lisiecki[2], Gregor Knorr[3], Sophie Nuber[1]†, Polychronis C. Tzedakis[4].

Affiliations:

[1]School of Earth and Environmental Sciences, Cardiff University; Cardiff, UK.

[2]Department of Earth Science, University of California; Santa Barbara, USA.

[3]Alfred Wegener Institute, Helmholtz Centre for Polar and Marine Research; Bremerhaven, Germany.

[4]Environmental Change Research Centre, Department of Geography, University College London; London, UK

*Corresponding author. Email: barkers3@cf.ac.uk

†Present address: Department of Oceanography, University of Washington; Washington, USA.

Abstract: Identifying the specific roles of precession, obliquity and eccentricity in glacial/interglacial transitions is hindered by imprecise age control. We circumvent this problem by focussing on the morphology of deglaciation/inception, which we show depends strongly on the relative phasing of precession versus obliquity. We demonstrate that while both parameters are important, precession has more influence on deglacial onset, while obliquity is more important for attainment of peak interglacial conditions and glacial inception. We find that the set of precession peaks (minima) responsible for terminations since 0.9Ma is a subset of those 'candidate peaks' which begin (precession parameter starts decreasing) while obliquity is increasing. Specifically, termination occurs with the first candidate peak following each eccentricity minimum. Thus the gross morphology of 100kyr glacial cycles appears largely deterministic.

Main Text:

Following demonstration that the succession of Quaternary ice ages is fundamentally controlled by changes in Earth's orbital geometry (*1*) many studies have attempted to identify the precise roles of precession, obliquity and eccentricity in the waxing and waning of continental ice sheets, in particular the process of glacial termination (deglaciation). The main obstacles to such an exercise include the closeness in frequency of precession (~1/21kyr) to the 2nd harmonic of obliquity (~1/20.5kyr) and the dating precision required to demonstrate a clear and reproducible link between either parameter and the end of a glacial period. Consequently, there has been considerable debate as to whether precession (*2-5*), obliquity (*6, 7*) or some combination of the two (*8-11*) provides the dominant driving force for glacial termination and moreover as to why glacial terminations tend to be separated by ~100kyr (one of the main periods of eccentricity), hence the '100kyr problem' (*2, 12, 13*). Here we take an alternative approach, based on the assumption that if precession and obliquity play distinct roles in deglaciation, then variations in their relative phasing will be imprinted on the trajectory of ice volume change across individual terminations.

As with previous studies of this type (e.g. *2, 3, 5, 6, 10, 14*) we utilise the record of benthic foraminiferal $\delta^{18}O$ to infer changes in continental ice volume while acknowledging that the signal is influenced by variations in deep ocean temperature (*15, 16*). Indeed, a lead in the timing of mean ocean warming ahead of ice volume decrease across the most recent deglaciation (Termination 1, T1) (*17*) implies a difference of ~2kyr between the $\delta^{18}O$ signal recorded by benthic foraminifera and the component of $\delta^{18}O$ related specifically to ice volume (*18*). However, as we show below, this offset is relatively small compared to the variations in morphology observed (several kyr). Additionally, it has been suggested that the record of benthic $\delta^{18}O$ can be considered a proxy for Earth's energy imbalance (the gain or loss of energy by the ocean-atmosphere system (*17*)) across intervals of ice sheet growth/decay and concomitant ocean cooling/warming (*18*). It could therefore be argued that the results reported here be interpreted in terms of the relative influences of precession and obliquity on Earth's energy imbalance associated with glacial/interglacial (G-IG) variability (see also Supplementary Material).

2. Quantifying deglacial morphology

We begin by quantifying the trajectory of benthic $\delta^{18}O$ across deglacial transitions and interglacials of the 100kyr world (approximately the last 800kyr; Figs. 1, 2). For this we use 3 independent stacks/records of benthic foraminiferal $\delta^{18}O$ (LR04/LR04_untuned (*14, 19*), HW04 (*20, 21*) and U1476pmag (*11*)) on 4 independent timescales (3 of which are free of orbital assumptions; See Methods (*16*)) to calculate the temporal offsets between 4 key points in the curve of $\delta^{18}O$ across each deglacial/interglacial period: (1) the onset of deglaciation (Onset deglac; when $\delta^{18}O$ begins to decrease following a glacial maximum (*16*)), (2) Max deglac: the point at which $\delta^{18}O$ reaches its maximum rate of decrease during termination, (3) Peak IG: the minimum in $\delta^{18}O$ associated with interglacial conditions and (4) Max inception: the subsequent maximum in the rate of $\delta^{18}O$ increase, marking a return to glacial conditions.

We do not define transitions between glacial and interglacial state based on a threshold in (e.g.) sea level or $\delta^{18}O$ (*10, 22*). Instead the points we select represent dynamical boundaries in the

curve of $\delta^{18}O$ (e.g. Peak IG represents the change from decreasing to increasing $\delta^{18}O$ while Max deglac represents the maximum rate of deglaciation). As previously suggested (*23*) this approach has the advantage of providing logical points in the climate curve that we might expect to align with maxima (or minima) in forcing (e.g. we may expect that the maximum rate of ice loss during deglaciation should correspond to a maximum in the forcing responsible). We nevertheless think it is useful to adhere to common nomenclature (e.g. for describing glacial versus interglacial periods). We therefore follow the traditional marine isotope stratigraphic definition of an interglacial as a broad minimum in $\delta^{18}O$ bounded by sharp transitions to heavier values (*24*), which in this case are delineated by Max deglac and Max inception. By this definition an interglacial is divided into a period of deglaciation and a period of glacial inception (Fig. 2A).

Our analysis suggests that variability in the total duration of deglaciation (from Onset deglac to Peak IG) is dominated by large (several kyr) changes in the offset between Max deglac and Peak IG (i.e. late deglaciation, which is equivalent to the deglacial phase of an interglacial; Figs. 1C; 2A) while the offset between Onset deglac and Max deglac (early deglaciation) is comparatively constant (8.6±1kyr for LR04 or 8.9±0.4kyr if Termination T8 is excluded, 7.8±0.9kyr for HW04 and 10±1.7kyr for U1476pmag; Fig. S2F). The interval between Peak IG and Max inception (the inception phase of an interglacial) is also relatively invariant (as previously observed (*25*)), with the offset between Max deglac and Max inception being strongly correlated to that between Max deglac and Peak IG (R^2 = 0.96/0.99 for LR04/LR04_untuned, R^2 = 0.87 for HW04, R^2 = 0.73 for U1476pmag; Figs. 2B, S4). From these results it can be seen that the entire duration from Onset deglac through to Max inception might be predicted simply from the offset between Max deglac and Peak IG.

3. Orbital phasing determines the duration of deglaciation

Previously (*25*) it was suggested that the phasing between precession and obliquity influences the persistence of interglacial conditions. Our results (Fig. 1) suggest that variations in interglacial duration (from Max deglac to Max inception) are dominated by changes in the deglacial phase (i.e. between Max deglac and Peak IG). We might therefore expect to find a relationship between orbital phasing and the offset from Max deglac to Peak IG. To test for such a relationship we need to quantify the phasing between precession and obliquity at the time of each deglaciation. To this end we identify the nearest precession peak to each deglacial transition (i.e. closest to Max deglac) and calculate the offset between that peak and its closest neighbouring peak in obliquity (Fig. 1D). Note that we use the term ‘peak’ (for both obliquity and precession) to describe conditions that give rise to a maximum in northern hemisphere summer insolation (which corresponds to a maximum in obliquity but a minimum in the precession parameter, when northern summer occurs during perihelion).

As stated, attempts to identify which orbital parameter might be more important for deglaciation have been limited by the requirement for accurate and precise age control of paleoproxy records. Our approach is much less sensitive to this requirement. Because we are looking for the closest precession peak to each deglaciation, the age models we employ are required only to have an accuracy of ~±10kyr (for comparison the stated uncertainties for LR04 and HW04 over the last 1Myr are ±4kyr and ±7kyr respectively). Accordingly the set of precession peaks identified for

the last 11 terminations within LR04 is exactly the same for all of the records/timescales analysed here (Fig. S2), giving us confidence in the robustness of our selection criteria.

The analysis reveals a strong correlation between Max deglac minus Peak IG and the phasing of precession versus obliquity (Figs. 2C, 2D, S3) with R^2 ranging from 0.74 to 0.88 for the various records and age models employed. Note that the alternative approach, of identifying the closest obliquity peak to Max deglac and its nearest neighbouring precession peak would give an equivalent result but with a negative slope (*16*) (Fig. S5). The observation of such a strong imprint of the phasing between obliquity and precession on the evolution of $\delta^{18}O$ across deglaciation implies not only that both parameters might play a role, but that these roles are somehow discrete (distinct), and therefore distinguishable.

4. Discrete roles for precession and obliquity in deglaciation and glacial inception

Previous studies have emphasised the importance of decreasing obliquity for glacial inception (*11, 25*). However, recent attempts to provide more precise constraints on the timing of glacial termination have reached different conclusions about the relative importance of obliquity versus precession for the onset of deglaciation (*5, 7*). Our results (Fig. 2) show that the duration from Max deglac through to Max inception is a linear function of the offset between peak precession and peak obliquity at the time of deglaciation. We suggest this implies that one parameter plays a more important role in the earlier stages of deglaciation (up to and including Max deglac) while the other is more influential on the latter stages and ultimately the subsequent glacial inception. To evaluate the alternative possibilities we compare 3 hypothetical scenarios (Figs. 3, 4).

In Scenario I we assume that the published age models for each record are accurate. This allows us to identify any significant relationships implied between each key point and the phase of precession or obliquity. For example, in Figure 3 we show results for two deglaciations (T2 and T5) with contrasting orbital phasing. We note that for T2, Max deglac is aligned (roughly) with maximum obliquity and decreasing precession (meaning that summers are intensifying). For T5, Max deglac is roughly aligned with peak (minimum) precession and rising obliquity. In both cases the subsequent Max inception is aligned with a positive precession parameter and low to minimum obliquity.

In Scenarios II and III we make the assumption that there should be a consistent relationship between Max deglac and the phase of whichever orbital parameter is responsible for the onset of deglaciation. Therefore in Scenario II we force Max deglac to align with the peak in precession closest to each termination and assess the implied alignment of Peak IG and Max inception with respect to the phase of obliquity. In Scenario III we align Max deglac with peak obliquity and assess the implied alignment of Peak IG and Max inception with respect to precession. We expect these implied alignments to be stronger when the correct starting parameter is selected, given the observed correlation between Max deglac - Peak IG versus orbital phasing. Our choice to set Max deglac to align with a peak in either parameter follows the logic that the maximum rate in ice volume decrease should coincide approximately with a maximum in forcing (*23*). On the other hand the exact phase employed is not critical for the arguments that follow, only that the phase is consistent for each termination.

For the example of T2 and T5 (Fig. 3) alignment of Max deglac with peak precession (Scenario II) results in alignment of Max inception with low to minimum obliquity in both cases i.e. Max

inception for T2 and T5 are aligned consistently with respect to the phase of obliquity, which would be expected if precession is the correct starting parameter. This is not the case for Scenario III, in which alignment of Max deglac with peak obliquity results in Max inception being aligned with a maximum or minimum in precession for T2 and T5 respectively (i.e. Max inception for T2 and T5 are not aligned consistently with respect to the phase of precession). From this limited example we would therefore select Scenario II as the most likely.

In Figure 4 we plot full results for each scenario for the 3 untuned age models over the last 1Myr (results including LR04 are given in Table S2). This interval includes 11 glacial terminations, but we exclude T1 because it has no subsequent inception. Results for Scenario I reveal a broad scatter of Max deglac around peaks in both obliquity and precession (Fig. 4A1, B1; S6A3, B3), suggesting (in keeping with previous studies (*5, 7, 8*)) that both parameters probably play some role in deglaciation. On the other hand obliquity alone seems to influence glacial inception, which is associated with decreasing to low obliquity (again consistent with previous work (*11, 25*)).

For scenarios II and III we use two approaches to assess the implied phasing between Peak IG (and Max inception) with respect to precession/obliquity (Methods (*16*)). Firstly we use the measured offsets between Max deglac and Peak IG (and Max inception) implied by the original age models. Secondly we predict those offsets from the relationships shown in Figures 2 (and S3, S4) based on the observed orbital phasing in each case. In Figure 4 we plot results using the second approach (full results are given in Table S2). Offsets between Onset deglac and Max deglac are measured in all cases.

In Scenario II we observe a strong alignment of Onset deglac with respect to precession (mean resultant vector length, $r = 0.87$, see Methods (*16*); Figs. 4A2, S6C2). This is not surprising given that the offset between Onset deglac and Max deglac is relatively constant (e.g. Fig.1C), but it is notable that the average offset (8.5±1.7kyr before the peak in precession) is just less than half a precession cycle, implying that if Max deglac coincides with peak precession then the onset of deglaciation occurs ~2kyr after northern summer insolation begins to intensify (as a function of precession). In this scenario Onset deglac and Max deglac also align with increasing to high values of obliquity (Figs. 4B2, S6D2,3). In fact we observe stronger alignment in these cases than observed in Scenario I ($r = 0.52$ vs 0.46 and $r = 0.54$ vs 0.44 respectively; Table S2). Thus for Scenario II the onset of deglaciation occurs when northern summer insolation is increasing as a function of both precession and obliquity (implying a dual role for obliquity and precession in the process of deglaciation).

The most outstanding result from Scenario II is the very strong alignment of Peak IG with decreasing obliquity (very close to the maximum rate of decrease) and of Max inception with low to minimum obliquity (Figs. 4B2, S6D4,5). In each case we obtain r values in excess of 0.95, much higher than those obtained in Scenario I (although the phase relationships observed are similar; Table S2). In other words, when Max deglac is set to peak precession, Peak IG and Max inception align precisely with respect to obliquity. Note that using the measured (rather than predicted) offsets between Max deglac and Peak IG (and Max inception) also gives r values greater than observed in Scenario I ($r = 0.82$ vs 0.64 and $r = 0.72$ vs 0.57 respectively; Table S2). The relationships between Peak IG and Max inception versus precession in Scenario II are not significant.

In Scenario III (Figs. 4B3, S6F3) we observe a strong alignment of Onset deglac with increasing obliquity (Fig. S6F2), analogous to Onset deglac versus precession in Scenario II. However, the relationships between Peak IG and Max inception versus precession are weak ($r < 0.4$) and although statistically significant for the combined records, this is not the case for any record when treated individually (Table S2). Notably in Scenario III, the relationships between Onset deglac and Max deglac versus precession are significantly worse than in Scenario I (Figs. 4A3, S6E2,3; Table S2) and imply that deglaciation is essentially independent of this parameter (i.e. no dual role for obliquity and precession in the process of deglaciation).

In summary, the results for Scenario II (in which Max deglac is aligned with peak precession) are consistent with a dual role for precession and obliquity in deglaciation and the proposition that precession plays a more important role in the precise timing of deglacial onset (*5*), while obliquity is more important for the timing of Peak IG and Max inception. The equivalent is not true for Scenario III. Setting Max deglac to peak obliquity does not result in strong alignment of Max inception with respect to precession and implies that no relationship exists between precession and deglaciation.

We note that while our conclusion (that precession is more important than obliquity for the onset of deglaciation) appears to contradict that of ref (*7*), both studies find that mid-deglaciation (Max deglac in our case) is aligned (approximately) with maximum summer insolation as a function of both obliquity and precession. Moreover, ref (*7*) noted a negative relationship between the value of obliquity at the onset of termination and the duration of termination. We suggest this reflects the fact that deglaciations tend to be longer when the peak to peak offset between precession and obliquity is greatest. For example the precession peak associated with T5 commenced while obliquity was close to minimum (Fig. 3B). This resulted in a very long (protracted) deglacial interval, reflecting the large phase offset at that time. In contrast, the precession peak associated with T2 commenced while obliquity was relatively high (i.e. precession and obliquity were close to being in phase; Fig. 3A), resulting in a much shorter period of deglaciation.

5. Importance of latitude for the waxing and waning of northern ice sheets

The combined effects of obliquity and precession (as modulated by eccentricity) on insolation are typically quantified using a single metric for example June 21 (peak northern summer) intensity or some measure of integrated summer insolation at 65°N. However, the relative contribution of obliquity versus precession to any given insolation metric decreases significantly as one moves from higher to lower latitudes (*11*) (Fig. 5A). Consequently, use of a single metric at a fixed latitude may be inadequate for defining the forcing relevant to an ice sheet whose mean latitude varies with time. Our results underscore this issue because they require that the relative importance of obliquity versus precession varies throughout a glacial cycle. Specifically, while precession appears to be more important for melting back very large ice sheets from their maximum extent, obliquity is more important for the end of glacial retreat and the beginning of the next glacial cycle. Glacial inception must occur at high latitude sites (north of ~70°N) such as the Canadian Arctic Archipelago (*26*). In these regions the contribution of obliquity to calorific summer insolation significantly outweighs that of precession (Fig. 5A). As ice sheets develop, their mean latitude will migrate southwards, to latitudes where precession is more important, until they attain their full glacial maximum position. At this point (anywhere south of ~55°N) precession dominates variations in both peak summer intensity and calorific summer insolation,

which can explain why the early stages of deglaciation are more strongly dependent on this parameter. Thereafter, as ice sheets decay, they retreat back toward higher latitudes where obliquity dominates (Fig. 5A).

Our inference (that precession is more important for the onset of deglaciation with obliquity more important for glacial inception) is supported by coupled climate-ice sheet model experiments. For example Abe-Ouchi et al. (*27*) demonstrated the sensitivity of very large ice sheets to even modest precession forcing at their southern margins, which could lead to their rapid disintegration during deglaciation. Vettoretti and Peltier (*28, 29*) emphasised the importance of obliquity for glacial inception, suggesting that occurrence of the Arctic insolation minimum in late spring, as a result of decreasing obliquity, led to delayed spring and summer snowmelt. Decreasing obliquity also increases the equator to pole insolation gradient during summer, which promotes northward moisture transport to feed growing icesheets (*29, 30*). On the other hand, other studies (*31, 32*) suggest that precession plays a more important role in glacial inception (as described in Section 7). In addition, conceptual models based on a limited number of tuneable parameters are able to simulate realistic timing of G-IG transitions using a single orbital solution (*33, 34*). Nevertheless, our results (Figs. 1, 2) clearly demonstrate the imprint of orbital phasing on deglaciation, which we contend is best explained by changes in the mean latitude and size of northern ice sheets and a corresponding change in their overall sensitivity to precession versus obliquity forcing.

So far, we have not considered the absolute magnitude of insolation forcing necessary for producing significant changes in ice sheet size. For example, the magnitude of precession forcing associated with T5 (leading to MIS 11) was small (a consequence of reduced eccentricity; Fig. 5B). And yet the magnitude of ice volume change across T5 was greater than terminations which experienced much larger variations in precession; hence, the 'Stage 11 problem' (*12, 35*). On the other hand, the vulnerability of very large ice sheets to even modest variations in precession might simply reflect their more southerly position (*27*) (Fig. 5B) or their inherent instability due to isostatic adjustments (*36*). In addition, feedbacks within the climate system play an important role in amplifying orbital forcing (*13, 37, 38*) and may therefore help to even out amplitude variations. For example, millennial-scale oscillations in ocean circulation and concomitant release of CO_2 during the early stages of termination can contribute to global warming at these times (*17, 39*). When ice sheets are particularly large (e.g. during MIS 12) it is possible that such feedbacks become substantial enough to compensate for potentially weaker precession forcing. Conversely, equivalent activity during glacial development may actually help to cool the deep ocean and provide additional storage capacity for lowering atmospheric CO_2 (*16, 38, 40*) (an essential aspect of glacial inception (*31*)).

It should be acknowledged that while our discussion has focussed on northern hemisphere ice sheet variability, fluctuations of the Antarctic ice sheet could account for a significant proportion (up to ~15%) of G-IG ice volume change (*41, 42*). We do not have a complete record of Antarctic ice sheet variability, but continuous temperature records do exist (*43, 44*). In Figure S7 we show a morphological comparison of the Antarctic temperature record (AAT) and the LR04 benthic stack over the past 800kyr. We observe a high degree of similarity ($R^2 = 0.93$) across deglaciations, implying (to first order) a common forcing.

Previous explanations of why Antarctic variability might resemble northern hemisphere insolation (which is counterintuitive, given that the effects of precession are out of phase

between the hemispheres (*45*)) have relied on interhemispheric 'bridges' such as sea level and atmospheric CO_2 (*13, 46*). Alternatively, it has been suggested that southern hemisphere summer duration (which varies in phase with northern summer intensity as a function of precession) could explain the similarity (*47*). On the other hand, our explanation for the shift in influence from precession to obliquity across (northern) deglaciation relies on a substantial change in the latitudinal distribution of ice, which is unlikely across Antarctica. Instead, we propose that precession could trigger the onset of deglacial Antarctic warming through heat redistribution associated with a substantial weakening of the Atlantic Meridional Overturning Circulation (AMOC) that might result from intensified summer melting of northern ice sheets (*37, 48-50*) and which in turn might be amplified by enhanced stratification of the glacial deep ocean (*39*). Notably, such an explanation could explain the observation of a southern lead at orbital timescales (*12, 51*), which would reflect the fact that deglacial warming across northern high latitudes is delayed by the same AMOC perturbations responsible for early warming in the south (*52, 53*).

An increase in the influence of obliquity towards the end of deglaciation in both hemispheres is more straightforward to explain thanks to the globally symmetric effects of obliquity.

6. Precession, obliquity and eccentricity combine to produce ~100kyr glacial cycles

The dominant ~100kyr period of mid/late Pleistocene G-IG cyclicity (*1*) is problematic because direct orbital forcing at this period (via eccentricity) is weak (*12*). Most recent studies have concluded that the large magnitude of glacial terminations must involve forcing by some combination of precession and/or obliquity with additional feedbacks internal to the climate system (*37*) and our results shed light on how these parameters combine to produce the observed morphology of deglacial/interglacial periods. However, there remains the question as to why glacial cycles should endure for so long and why they have such a strong link to eccentricity (*14*) (Fig. 5B). Raymo (*2*) suggested that an extended interval of low amplitude precession forcing (under the influence of low eccentricity) would allow the build-up of large continental ice sheets by enabling them to expand southwards until they reached some critical size, after which they would become susceptible to even modest insolation forcing. Accordingly, most successful models of G-IG variability (*8, 9, 13, 34, 54*) incorporate a critical ice volume threshold (V_{crit}), beyond which termination becomes possible/inevitable.

Our results provide empirical constraints for predicting the occurrence and duration of glacial terminations and interglacials since the Mid Pleistocene Transition (MPT i.e. the 100kyr world; Fig. 6). As stated, the set of precession peaks associated with Max deglac for each termination of the past 1Myr is identical for all of the $\delta^{18}O$ records analysed here (Fig. S2). Furthermore, each of those peaks was aligned with average to high values of obliquity (Fig. 1D, E), which implies that obliquity was rising as peak summer intensity began increasing as a function of precession (see orange symbols in Fig. 1D, E). This is true for all terminations except T8, whose precession peak begins ~724ka, about 1kyr before the next minimum in obliquity (Fig. 1D, E) and therefore about 2kyr before obliquity starts to rise. Notably, according to 3 out of 4 $\delta^{18}O$ records, the measured offset between Onset deglac and Max deglac associated with T8 is shorter than the average (Fig. S2). This is particularly noticeable for LR04 (Fig. 1C) and we speculate that this is due to the relatively late (~2kyr) rise in obliquity associated with that termination. We therefore

consider precession peaks as candidates for termination if they begin while obliquity is rising or begins rising within 2kyr of the turning point in precession (to accommodate the case of T8). Thus the onset of deglaciation occurred only when summers were warming through the reinforcing (dual) effects of obliquity and precession (see also results in Fig. 4). In Figure 6H we plot all such 'candidate' precession peaks of the past 1Myr.

Significantly the subset of candidate precession peaks resulting in termination over the past 900kyr is precisely those that directly followed a minimum in eccentricity (Fig. 6H; note that the eccentricity minimum ~373Ka coincided precisely with a candidate precession peak but the following candidate peak was the terminating peak). For context, there have been 45 precession peaks since 0.95Ma, of which 25 (~1/2) were candidate peaks and just 10 (1/4.5) were associated with glacial termination (i.e. on average terminations were separated by 4.5 precession cycles, ~95kyr).

Glacial termination therefore occurs with the first candidate precession peak following each minimum in eccentricity. This might suggest that V_{crit} is attained as soon as eccentricity reaches its minimum, after which the next candidate peak in precession triggers deglaciation. However, we note that in many cases, one or more non-candidate precession peaks occurred within the interval between the minimum in eccentricity and the terminating precession peak. Since non-candidate precession peaks are (by definition) those that align with low obliquity, continued ice growth during these intervals might also be critical for attainment of V_{crit} prior to termination (*13*). In any case, our observations allow us to construct an algorithm capable of predicting the occurrence of all major glacial terminations over the past 900kyr, based simply on the subset of candidate precession peaks that follow directly after minima in eccentricity (Fig. 6H). In Figure 6D we also incorporate predictions for the key points (Peak IG and Max inception), based on the phasing of precession versus obliquity during termination.

The results compare well with those obtained from a simple thresholding approach used to predict interglacial stages of the past 1Myr (*10*) (Fig. 6I), with three exceptions: In two cases, our algorithm does not predict the transitions into marine isotope substages 7c or 15a. While these events were aligned with candidate peaks (Fig. 6G), they were relatively short in duration with respect to the phasing of precession versus obliquity (Fig. 2C, D) and do not fall within the set of major terminations. Notably though, they occurred when the amplitude of precession forcing was particularly large (thanks to high eccentricity). We therefore consider MIS 7c and 15a as anomalously warm substages, analogous to MIS 5a and 9a (Fig 6G) but of larger amplitude thanks to the direct influence of eccentricity on precession. In the third case, T6 was a protracted (2-step) termination (*55*), resulting in the delayed attainment of full interglacial conditions (MIS 13a) according to the prediction of (*10*). The preceding glacial (MIS 14) was particularly weak (*56*) and the smaller size of ice sheets (Fig. 6G) might explain the weaker response to orbital forcing associated with the first step (T6). The second step (T6a) was also aligned with a candidate precession peak and its duration (relative to orbital phasing) was in line with all other major terminations (Fig. 2C, D). Thus the full deglaciation from MIS 14 into MIS 13a could be considered as 2 distinct deglacial events, each following the pattern of other major terminations of the past 900kyr.

Our simple rules for predicting the occurrence of terminating precession peaks do not hold prior to 0.9Ma (Figs. 6, S8). Notably, this was during the Mid Pleistocene Transition (~1.2 to 0.8Ma (*57-61*)) before which glacial cycles had a period of ~41kyr, similar to that of obliquity. At that

time, according to the records and age models used here, deglacial transitions were also more closely aligned with candidate precession peaks (i.e. those that commenced while obliquity was increasing) than with non-candidate peaks, with almost all candidate peaks being associated with a deglacial event (Fig. S8), which is in contrast to the 100kyr world (Fig. 6). This does not necessarily imply that precession was critical for deglacial transitions before the MPT because our definition of a candidate precession peak is one that coincides with moderate to high obliquity (which therefore could be solely responsible for pre-MPT deglaciations). On the other hand, it does imply that eccentricity had little influence on the duration of glacial periods prior to the MPT. We might therefore explain the change from ~41 to ~100kyr glacial periodicity across the MPT as resulting from the increasing ability of ice sheets to grow and/or expand southwards quickly enough to escape the influence of obliquity (e.g. by secular global cooling, changes in glacial erosion or an increase in moisture transport associated with the Atlantic Inflow (*10, 11, 59, 60, 62, 63*)), while simultaneously escaping the influence of precession thanks to decreasing eccentricity (*2, 54*). Eventually though, ice sheets would reach a latitude and size where even a modest change in precession could trigger glacial termination (*27, 36*). Thus the MPT saw the introduction of a dependency on eccentricity, but crucially this was not associated with maxima in eccentricity but rather minima, providing the necessary time required to grow very large ice sheets (*2, 10, 34, 54*).

Finally, we note that ~100kyr periodicity has also been observed for glacial cycles during earlier epochs, for example the early to mid Miocene (*64, 65*). At that time, continental ice was most likely confined to Antarctica (*66*) and while the mechanisms we invoke to explain ~100kyr periodicity during the Pleistocene are focused on northern hemisphere processes, future work should investigate whether or not equivalent mechanisms involving the Antarctic ice sheet could be called upon during earlier intervals. Notably, the potential importance of millennial-scale variability and its possible interactions with orbital timescale changes has been invoked for the Miocene (*67*) as well as the mid to late Pleistocene (*37, 38*).

7. The natural future of Earth's climate

Our results suggest that the succession and duration of deglacial/interglacial events since the MPT might be largely determined by the relative phasing of precession, obliquity and eccentricity (Fig. 6D). This deterministic quality (previously inferred from theoretical/model-based approaches (*9, 68, 69*)) provides an opportunity to hypothesise about the possible future of Earth's climate. There has been considerable discussion as to when the next glacial inception might occur (*29, 31, 32, 70*). Most studies agree that glacial inception results from some critical combination of orbital configuration and the atmospheric concentration of CO_2 and there is little debate that while CO_2 levels continue to rise there is almost no chance of a return to glacial conditions (*29, 31*). Notwithstanding, it is important to understand the natural variability of climate and how this might play out if and when the anthropogenic input of CO_2 is reduced to pre-industrial levels. Classical orbital theory predicts that glacial inception should occur when northern hemisphere summers are cool enough to allow perennial snow to accumulate, through some combination of low obliquity and a positive precession parameter (when northern summer aligns with aphelion). Orbital eccentricity (the circularity of Earth's orbit around the Sun) is currently low ($e \approx 0.017$ compared with a maximum of ~0.58), resulting in very modest variations in precession (Figs. 6, 7). Consequently, model predictions based on the intensity of

peak summer insolation at 65°N (a signal dominated by precession) tend to escape inception for tens of thousands of years into the future even in the hypothetical absence of anthropogenic CO_2 (*31, 32*). On the other hand, models that emphasize the importance of obliquity (over precession) in the process of inception (*28, 29*) predict glacial inception as early as 10kyr from now (with CO_2 held at 260ppmv).

Our results also suggest that glacial inception depends mainly on the phase of obliquity, and moreover that the duration between Peak IG and Max inception is rather invariant (Fig. 2B) and therefore relatively insensitive to the amplitude of precession forcing. For example, eccentricity was also low across T5 (as discussed above) and although MIS 11 was long, it fell within the natural set of mid to late Pleistocene interglacials whose durations were dictated by the phasing of precession versus obliquity during deglaciation (i.e. it was not exceptional; Fig. 7A). Conversely, MIS 7e was relatively short and occurred when eccentricity was high, but its short duration could again be predicted simply from the negative peak-to-peak offset between precession and obliquity across T3 (Fig. 7B). MIS 19 (following T9), which is often taken as an analogue for our current interglacial (MIS 1) because it experienced similar variations in insolation (*70*) (i.e. low eccentricity with precession and obliquity approximately in-phase during deglaciation), also had a duration in keeping with predictions based on orbital phasing rather than eccentricity (Fig. 7C).

We therefore calculate when the next maximum in glacial inception might occur (ignoring the effects of anthropogenic CO_2) based on the phasing of precession versus obliquity during the last deglaciation (T1). According to the various records we employ, benthic $\delta^{18}O$ has continued to decrease throughout the Holocene, which results in an age of zero being assigned to MIS 1 Peak IG (Fig. 7D) although we cannot know whether or not this the actual minimum because there is no record of the future. We therefore predict the timing of MIS 1 Peak IG from the empirical relationships shown in Figure 2 (and S3) while omitting T1. We set Max deglac for each record either to the age of Max deglac on LR04 (which is based on ^{14}C dating (*19*); Set L in Fig. 7D) or the precession peak ~11ka (Set P in Fig. 7D) (*16*). We then use the calculated values of Max deglac minus Peak IG to estimate the age of Max inception. We obtain an age of -0.1±1.8kyr (2σ) for MIS 1 Peak IG and -7.7±3.4kyr (2σ) for the next Max inception. Thus we estimate that, if not for the effects of increasing CO_2, glacial inception would reach a maximum rate within the next 11kyr, as obliquity decreases towards its next minimum.

Our extrapolation also suggests that the next interglacial event would begin ~66kyr from now (following a glacial cycle spanning 4 precession peaks; Fig. 6D). The same timing is predicted by the simple rules outlined in ref (*10*) (Fig. 6). On the other hand, while atmospheric CO_2 remains above pre-industrial levels it is highly unlikely that glacial inception will occur (*29, 31, 71*), in which case the pattern of future interglacials will be very different from the predictions made here.

References and Notes

1. J. D. Hays, J. Imbrie, N. J. Shackleton, Variations in the Earth's orbit: Pacemaker of the Ice Ages. *Science* **194**, 1121-1132 (1976).

2. M. E. Raymo, The timing of major climate terminations. *Paleoceanography* **12**, 577-585 (1997).
3. A. J. Ridgwell, A. J. Watson, M. E. Raymo, Is the spectral signature of the 100 kyr glacial cycle consistent with a Milankovitch origin? *Paleoceanography* **14**, 437-440 (1999).
4. H. Cheng, R. L. Edwards, A. Sinha, C. Spötl, L. Yi, S. Chen, M. Kelly, G. Kathayat, X. Wang, X. Li, The Asian monsoon over the past 640,000 years and ice age terminations. *Nature* **534**, 640-646 (2016).
5. B. Hobart, L. E. Lisiecki, D. Rand, T. Lee, C. E. Lawrence, Late Pleistocene 100-kyr glacial cycles paced by precession forcing of summer insolation. *Nature Geoscience* **16**, 717-722 (2023).
6. P. Huybers, C. Wunsch, Obliquity pacing of the late Pleistocene glacial terminations. *Nature* **434**, 491-494 (2005).
7. P. Bajo, R. N. Drysdale, J. D. Woodhead, J. C. Hellstrom, D. Hodell, P. Ferretti, A. H. Voelker, G. Zanchetta, T. Rodrigues, E. Wolff, Persistent influence of obliquity on ice age terminations since the Middle Pleistocene transition. *Science* **367**, 1235-1239 (2020).
8. P. Huybers, Combined obliquity and precession pacing of late Pleistocene deglaciations. *Nature* **480**, 229-232 (2011).
9. F. Parrenin, D. Paillard, Terminations VI and VIII (∼ 530 and∼ 720 kyr BP) tell us the importance of obliquity and precession in the triggering of deglaciations. *Climate of the Past* **8**, 2031-2037 (2012).
10. P. C. Tzedakis, M. Crucifix, T. Mitsui, E. W. Wolff, A simple rule to determine which insolation cycles lead to interglacials. *Nature* **542**, 427-432 (2017).
11. S. Barker, A. Starr, J. v. d. Lubbe, A. Doughty, G. Knorr, S. Conn, S. Lordsmith, L. Owen, A. Nederbragt, S. Hemming, I. Hall, L. Levay, Persistent influence of precession on northern ice sheet variability since the early Pleistocene. *Science* **376**, 961-967 (2022) doi: 10.1126/science.abm4033.
12. J. Imbrie, A. Berger, E. A. Boyle, S. C. Clemens, A. Duffy, W. R. Howard, G. Kukla, J. Kutzbach, D. G. Martinson, A. McIntyre, A. C. Mix, B. Molfino, J. J. Morley, L. C. Peterson, N. G. Pisias, W. L. Prell, M. E. Raymo, N. J. Shackleton, J. R. Toggweiler, On the structure and origin of major glaciation cycles 2. the 100,000-year cycle. *Paleoceanography* **8**, 699-735 (1993).
13. A. Ganopolski, Toward generalized Milankovitch theory (GMT). *Climate of the Past* **20**, 151-185 (2024).
14. L. E. Lisiecki, Links between eccentricity forcing and the 100,000-year glacial cycle. *Nature geoscience* **3**, 349-352 (2010).
15. H. Elderfield, P. Ferretti, M. Greaves, S. Crowhurst, I. N. McCave, D. Hodell, A. M. Piotrowski, Evolution of Ocean Temperature and Ice Volume Through the Mid-Pleistocene Climate Transition. *Science* **337**, 704-709 (2012).
16. See Supplementary Materials.
17. D. Baggenstos, M. Häberli, J. Schmitt, S. A. Shackleton, B. Birner, J. P. Severinghaus, T. Kellerhals, H. Fischer, Earth's radiative imbalance from the Last Glacial Maximum to the present. *Proceedings of the National Academy of Sciences* **116**, 14881-14886 (2019).
18. S. Shackleton, A. Seltzer, D. Baggenstos, L. E. Lisiecki, Benthic δ18O records Earth's energy imbalance. *Nature Geoscience* **16**, 797-802 (2023).
19. L. E. Lisiecki, M. E. Raymo, A Pliocene-Pleistocene stack of 57 globally distributed benthic $\delta^{18}O$ records. *Paleoceanography* **20**, DOI:10.1029/2004PA001071 (2005).

20. P. Huybers, C. Wunsch, A depth-derived Pleistocene age model: Uncertainty estimates, sedimentation variability, and nonlinear climate change. *Paleoceanography* **19**, (2004).
21. P. Huybers, Glacial variability over the last two million years: an extended depth-derived agemodel, continuous obliquity pacing, and the Pleistocene progression. *Quaternary Science Reviews* **26**, 37-55 (2007).
22. PIGS_of_PAGES, Interglacials of the last 800,000 years. *Reviews of Geophysics* **54**, 162-219 (2016).
23. G. Roe, In defense of Milankovitch. *Geophysical Research Letters* **33**, (2006) 10.1029/2006GL027817.
24. N. J. Shackleton, N. D. Opdyke, Oxygen isotope and palaeomagnetic stratigraphy of Equatorial Pacific core V28-238: Oxygen isotope temperatures and ice volumes on a 105 year and 106 year scale. *Quaternary Research* **3**, 39-55 (1973).
25. P. C. Tzedakis, E. Wolff, L. Skinner, V. Brovkin, D. Hodell, J. F. McManus, D. Raynaud, Can we predict the duration of an interglacial? *Climate of the Past* **8**, 1473-1485 (2012).
26. P. Clark, J. Clague, B. B. Curry, A. Dreimanis, S. Hicock, G. Miller, G. Berger, N. Eyles, M. Lamothe, B. Miller, Initiation and development of the Laurentide and Cordilleran ice sheets following the last interglaciation. *Quaternary Science Reviews* **12**, 79-114 (1993).
27. A. Abe-Ouchi, F. Saito, K. Kawamura, M. E. Raymo, J. i. Okuno, K. Takahashi, H. Blatter, Insolation-driven 100,000-year glacial cycles and hysteresis of ice-sheet volume. *Nature* **500**, 190-193 (2013).
28. G. Vettoretti, W. R. Peltier, Sensitivity of glacial inception to orbital and greenhouse gas climate forcing. *Quaternary Science Reviews* **23**, 499-519 (2004).
29. G. Vettoretti, W. Peltier, The impact of insolation, greenhouse gas forcing and ocean circulation changes on glacial inception. *The Holocene* **21**, 803-817 (2011).
30. M. E. Raymo, K. Nisancioglu, The 41 kyr world: Milankovitch's other unsolved mystery. *Paleoceanography* **18**, (2003) 10.1029/2002PA000791.
31. A. Ganopolski, R. Winkelmann, H. J. Schellnhuber, Critical insolation–CO2 relation for diagnosing past and future glacial inception. *Nature* **529**, 200-203 (2016).
32. A. Berger, M. F. Loutre, An exceptionally long interglacial ahead? *Science* **297**, 1287-1288 (2002).
33. F. Parrenin, D. Paillard, Amplitude and phase of glacial cycles from a conceptual model. *Earth and Planetary Science Letters* **214**, 243-250 (2003).
34. E. Legrain, F. Parrenin, E. Capron, A gradual change is more likely to have caused the mid-pleistocene transition than an abrupt event. *Communications Earth & Environment* **4**, 90 (2023).
35. P. C. Tzedakis, D. A. Hodell, C. Nehrbass-Ahles, T. Mitsui, E. W. Wolff, Marine isotope stage 11c: An unusual interglacial. *Quaternary Science Reviews* **284**, 107493 (2022).
36. D. R. MacAyeal, A Catastrophe Model of the Paleoclimate. *Journal of Glaciology* **24**, 245-257 (1979).
37. S. Barker, G. Knorr, Millennial scale feedbacks determine the shape and rapidity of glacial termination. *Nature Communications* **12**, 2273 (2021) 10.1038/s41467-021-22388-6.
38. S. Barker, G. Knorr, A Systematic Role for Extreme Ocean-Atmosphere Oscillations in the Development of Glacial Conditions Since the Mid Pleistocene Transition. *Paleoceanography and Paleoclimatology* **38**, (2023) 10.1029/2023PA004690.

39. G. Knorr, S. Barker, X. Zhang, G. Lohmann, X. Gong, P. Gierz, C. Stepanek, L. B. Stap, A salty deep ocean as a prerequisite for glacial termination. *Nature Geoscience* **14**, 930-936 (2021).
40. S. Shackleton, J. A. Menking, E. Brook, C. Buizert, M. N. Dyonisius, V. V. Petrenko, D. Baggenstos, J. P. Severinghaus, Evolution of mean ocean temperature in Marine Isotope Stage 4. *Climate of the Past* **17**, 2273-2289 (2021).
41. R. M. DeConto, D. Pollard, Contribution of Antarctica to past and future sea-level rise. *Nature* **531**, 591-597 (2016).
42. N. R. Golledge, R. H. Levy, R. M. McKay, C. J. Fogwill, D. A. White, A. G. Graham, J. A. Smith, C.-D. Hillenbrand, K. J. Licht, G. H. Denton, Glaciology and geological signature of the Last Glacial Maximum Antarctic ice sheet. *Quaternary Science Reviews* **78**, 225-247 (2013).
43. J. Jouzel, V. Masson-Delmotte, O. Cattani, G. Dreyfus, S. Falourd, G. Hoffmann, B. Minster, J. Nouet, J. M. Barnola, J. Chappellaz, H. Fischer, J. C. Gallet, S. Johnsen, M. Leuenberger, L. Loulergue, D. Luethi, H. Oerter, F. Parrenin, G. Raisbeck, D. Raynaud, A. Schilt, J. Schwander, E. Selmo, R. Souchez, R. Spahni, B. Stauffer, J. P. Steffensen, B. Stenni, T. F. Stocker, J. L. Tison, M. Werner, E. W. Wolff, Orbital and millennial Antarctic climate variability over the past 800,000 years. *Science* **317**, 793-796 (2007).
44. F. Parrenin, V. Masson-Delmotte, P. Kohler, D. Raynaud, D. Paillard, J. Schwander, C. Barbante, A. l. Landais, A. Wegner, J. Jouzel, Synchronous change of atmospheric CO_2 and Antarctic temperature during the last deglacial warming. *Science* **339**, 1060-1063 (2013).
45. J. H. Mercer, in *Climate Processes and Climate Sensitivity,* J. E. Hansen, Takahash.T, Eds. (American Geophysical Union, 1984), vol. 29, pp. 307-313.
46. T. T. Barrows, S. Juggins, P. De Deckker, E. Calvo, C. Pelejero, Long-term sea surface temperature and climate change in the Australian–New Zealand region. *Paleoceanography* **22**, (2007).
47. P. Huybers, G. Denton, Antarctic temperature at orbital timescales controlled by local summer duration. *Nature Geoscience* **1**, 787-792 (2008).
48. S. Barker, P. Diz, M. J. Vautravers, J. Pike, G. Knorr, I. R. Hall, W. S. Broecker, Interhemispheric Atlantic seesaw response during the last deglaciation. *Nature* **457**, 1097-1102 (2009).
49. E. W. Wolff, H. Fischer, R. Rothlisberger, Glacial terminations as southern warmings without northern control. *Nature Geoscience* **2**, 206-209 (2009).
50. G. H. Denton, R. F. Anderson, J. R. Toggweiler, R. L. Edwards, J. M. Schaefer, A. E. Putnam, The Last Glacial Termination. *Science* **328**, 1652-1656 (2010).
51. C. Wunsch, Greenland - Antarctic phase relations and millennial time-scale climate fluctuations in the Greenland ice-cores. *Quaternary Science Reviews* **22**, 1631-1646 (2003).
52. S. Barker, G. Knorr, R. L. Edwards, F. Parrenin, A. E. Putnam, L. C. Skinner, E. Wolff, M. Ziegler, 800,000 years of abrupt climate variability. *Science* **334**, 347-351 (2011).
53. J. D. Shakun, P. U. Clark, F. He, S. A. Marcott, A. C. Mix, Z. Liu, B. Otto-Bliesner, A. Schmittner, E. Bard, Global warming preceded by increasing carbon dioxide concentrations during the last deglaciation. *Nature* **484**, 49-54 (2012).
54. D. Paillard, The timing of Pleistocene glaciations from a simple multiple-state climate model. *Nature* **391**, 378 (1998).

55. S. Barker, G. Knorr, S. Conn, S. Lordsmith, D. Newman, D. Thornalley, Early interglacial legacy of deglacial climate instability. *Paleoceanography and Paleoclimatology*, (2019) 10.1029/2019PA003661.
56. N. Lang, E. W. Wolff, Interglacial and glacial variability from the last 800 ka in marine, ice and terrestrial archives. *Climate of the Past* **7**, 361 (2011).
57. N. J. Shackleton, N. D. Opdyke, Oxygen-isotope and paleomagnetic stratigraphy of Pacific core V28-239 late Pliocene to latest Pleistocene. (1976).
58. N. G. Pisias, T. Moore Jr, The evolution of Pleistocene climate: a time series approach. *Earth and Planetary Science Letters* **52**, 450-458 (1981).
59. P. U. Clark, D. Archer, D. Pollard, J. D. Blum, J. A. Rial, V. Brovkin, A. C. Mix, N. G. Pisias, M. Roy, The middle Pleistocene transition: characteristics. mechanisms, and implications for long-term changes in atmospheric PCO2. *Quaternary Science Reviews* **25**, 3150-3184 (2006).
60. S. Barker, X. Zhang, L. Jonkers, S. Lordsmith, S. Conn, G. Knorr, Strengthening Atlantic Inflow across the Mid-Pleistocene Transition. *Paleoceanography and Paleoclimatology*, (2021) 10.1029/2020PA004200.
61. P. U. Clark, D. Pollard, Origin of the middle Pleistocene transition by ice sheet erosion of regolith. *Paleoceanography* **13**, 1-9 (1998).
62. W. H. Berger, E. Jansen, in *The polar oceans and their role in shaping the global environment*. (AGU, 1994), pp. 295-311.
63. E. L. McClymont, S. M. Sosdian, A. Rosell-Melé, Y. Rosenthal, Pleistocene sea-surface temperature evolution: Early cooling, delayed glacial intensification, and implications for the mid-Pleistocene climate transition. *Earth-Science Reviews* **123**, 173-193 (2013).
64. D. Liebrand, L. Lourens, D. Hodell, B. De Boer, R. Van de Wal, H. Pälike, Antarctic ice sheet and oceanographic response to eccentricity forcing during the early Miocene. *Climate of the Past* **7**, 869-880 (2011).
65. A. Holbourn, W. Kuhnt, K. G. Kochhann, N. Andersen, K. Sebastian Meier, Global perturbation of the carbon cycle at the onset of the Miocene Climatic Optimum. *Geology* **43**, 123-126 (2015).
66. J. Zachos, M. Pagani, L. Sloan, E. Thomas, K. Billups, Trends, rhythms, and aberrations in global climate 65 Ma to present. *Science* **292**, 686-693 (2001).
67. N. B. Sullivan, S. R. Meyers, R. H. Levy, R. M. McKay, N. R. Golledge, G. Cortese, Millennial-scale variability of the Antarctic ice sheet during the early Miocene. *Proceedings of the National Academy of Sciences* **120**, e2304152120 (2023).
68. M. Willeit, A. Ganopolski, R. Calov, V. Brovkin, Mid-Pleistocene transition in glacial cycles explained by declining CO2 and regolith removal. *Science Advances* **5**, eaav7337 (2019).
69. S. R. Meyers, L. A. Hinnov, Northern Hemisphere glaciation and the evolution of Plio-Pleistocene climate noise. *Paleoceanography* **25**, (2010).
70. P. C. Tzedakis, J. Channell, D. Hodell, H. Kleiven, L. Skinner, Determining the natural length of the current interglacial. *Nature Geoscience* **5**, 138-141 (2012).
71. D. Archer, A. Ganopolski, A movable trigger: Fossil fuel CO2 and the onset of the next glaciation. *Geochemistry Geophysics Geosystems* **6**, (2005).
72. A. Berger, M. F. Loutre, Insolation Values for the Climate of the Last 10 Million Years. *Quaternary Science Reviews* **10**, 297-317 (1991).
73. M. Crucifix, Palinsol: insolation for palaeoclimate studies, R package version 0.93. https://bitbucket.org/mcrucifix/insol (2016).

74. C. Waelbroeck, J. C. Duplessy, E. Michel, L. Labeyrie, D. Paillard, J. Duprat, The timing of the last deglaciation in North Atlantic climate records. *Nature* **412**, 724-727 (2001).
75. N. J. Shackleton, M. A. Hall, E. Vincent, Phase relationships between millennial-scale events 64,000- 24,000 years ago. *Paleoceanography* **15**, 565-569 (2000).
76. R. B. Alley, E. J. Brook, S. Anandakrishnan, A northern lead in the orbital band: north-south phasing of Ice-Age events. *Quaternary Science Reviews* **21**, 431-441 (2002).
77. A. Schmittner, O. A. Saenko, A. J. Weaver, Coupling of the hemispheres in observations and simulations of glacial climate change. *Quaternary Science Reviews* **22**, 659-671 (2003).
78. S. Barker, G. Knorr, Antarctic climate signature in the Greenland ice core record. *Proceedings of the National Academy of Sciences of the United States of America* **104**, 17278-17282 (2007).
79. L. Skinner, N. Shackleton, Deconstructing Terminations I and II: revisiting the glacioeustatic paradigm based on deep-water temperature estimates. *Quaternary Science Reviews* **25**, 3312-3321 (2006).
80. D. M. Sigman, M. P. Hain, G. H. Haug, The polar ocean and glacial cycles in atmospheric CO_2 concentration. *Nature* **466**, 47-55 (2010).
81. J. F. Adkins, The role of deep ocean circulation in setting glacial climates. *Paleoceanography* **28**, 539-561 (2013).
82. P. Berens, CircStat: a MATLAB toolbox for circular statistics. *J Stat Softw* **31**, 1-21 (2009).
83. J. V. Stern, L. E. Lisiecki, Termination 1 timing in radiocarbon-dated regional benthic δ18O stacks. *Paleoceanography* **29**, 1127-1142 (2014).
84. B. Bereiter, S. Shackleton, D. Baggenstos, K. Kawamura, J. Severinghaus, Mean global ocean temperatures during the last glacial transition. *Nature* **553**, 39 (2018).
85. K. Lambeck, H. Rouby, A. Purcell, Y. Sun, M. Sambridge, Sea level and global ice volumes from the Last Glacial Maximum to the Holocene. *Proceedings of the National Academy of Sciences* **111**, 15296-15303 (2014).
86. L. Bazin, A. Landais, B. Lemieux-Dudon, H. Toyé Mahamadou Kele, D. Veres, F. Parrenin, P. Martinerie, C. Ritz, E. Capron, V. Lipenkov, An optimized multi-proxy, multi-site Antarctic ice and gas orbital chronology (AICC2012): 120-800 ka. *Climate of the Past* **9**, 1715-1731 (2013).
87. D. Veres, L. Bazin, A. Landais, H. ToyÃ© Mahamadou Kele, B. Lemieux-Dudon, F. Parrenin, P. Martinerie, E. Blayo, T. Blunier, E. Capron, The Antarctic ice core chronology (AICC2012): an optimized multi-parameter and multi-site dating approach for the last 120 thousand years. *Climate of the Past Discussions* **8**, 6011-6049 (2012).

Acknowledgments: We thank M. Crucifix for assistance with palinsol. This is Cardiff EARTH CRediT contribution 26. **Author contributions:** Conceptualization: SB, LEL, GK, PCT; Methodology: SB; Investigation: SB; Visualization: SB; Writing – original draft: SB, LEL, GK, PCT ; Writing – review & editing: SB, LEL, GK, SN, PCT. **Competing interests:** Authors declare that they have no competing interests. **Data and materials availability:** All data used in this study were published previously and readers are referred to the references listed within supplementary materials. All analyses used in this study are described in the supplementary materials.

Supplementary Materials

Materials and Methods

Figs. S1 to S9

Tables S1 to S2

References (74-87)

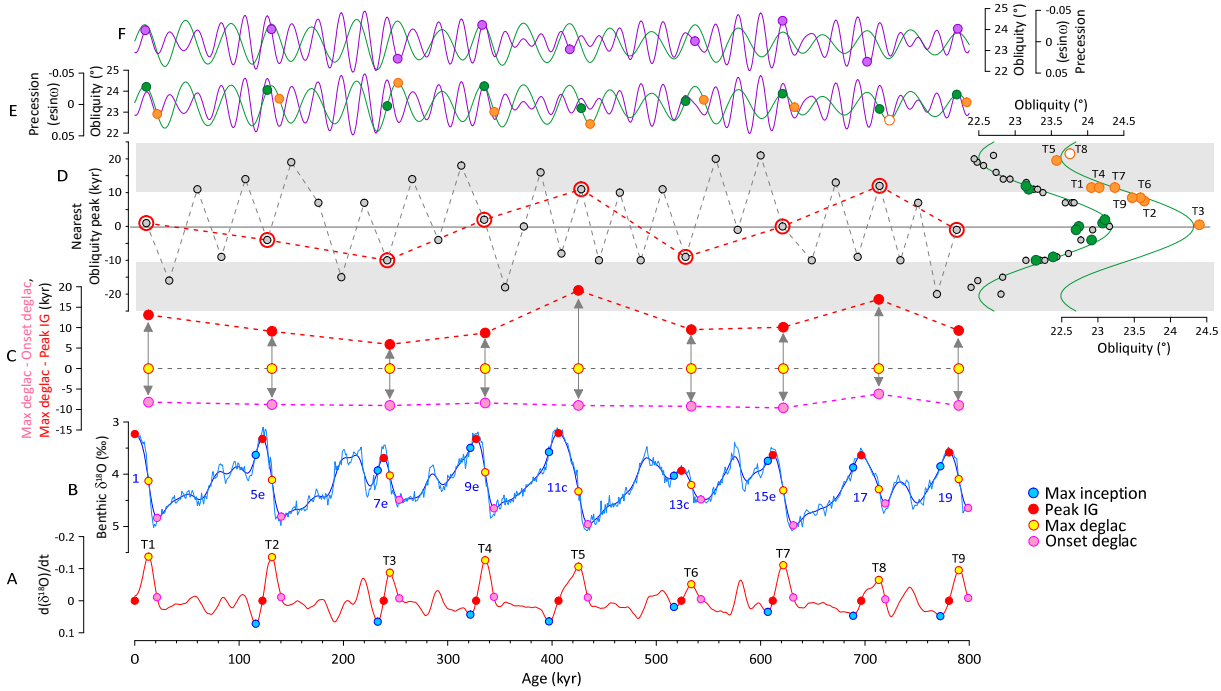

Fig. 1. Deglacial morphology and the phasing of obliquity versus precession. (A, B) The LR04 benthic $\delta^{18}O$ stack (B) and its first derivative (A), used to identify the key points as described in main text (coloured symbols). Terminations are numbered T1-T9, MIS numbers in blue. (C) Calculated temporal offsets: Max deglac minus Onset deglac (pink symbols), Max deglac minus Peak IG (red). Variability in the duration of deglaciation (double-headed grey arrows) is dominated by changes in the offset between Max deglac and Peak IG. (D) Precession peaks plotted versus their temporal offset to the closest obliquity peak in each case. Large red symbols (joined by dashed lines) are those precession peaks that are closest to Max deglac in each case. All of these coincide with moderate to high values of obliquity as demonstrated by green symbols to right. Also plotted is the value of obliquity (orange symbols) associated with the beginning of each terminal precession peak (i.e. when the precession parameter shifts from increasing to decreasing; see also Part E and discussion in Section 6). (E) Precession and obliquity (*72*) over last 1Myr. Green symbols highlight value of obliquity at each terminal precession peak, orange symbols highlight phase of obliquity at the beginning of each terminal precession peak (increasing in all cases except T8, which starts to increase within 2kyr; see text). (F) Same as E but purple symbols reflect value of precession parameter for the closest obliquity maximum to each Max deglaciation (no systematic pattern is observed cf. Fig. S6E3).

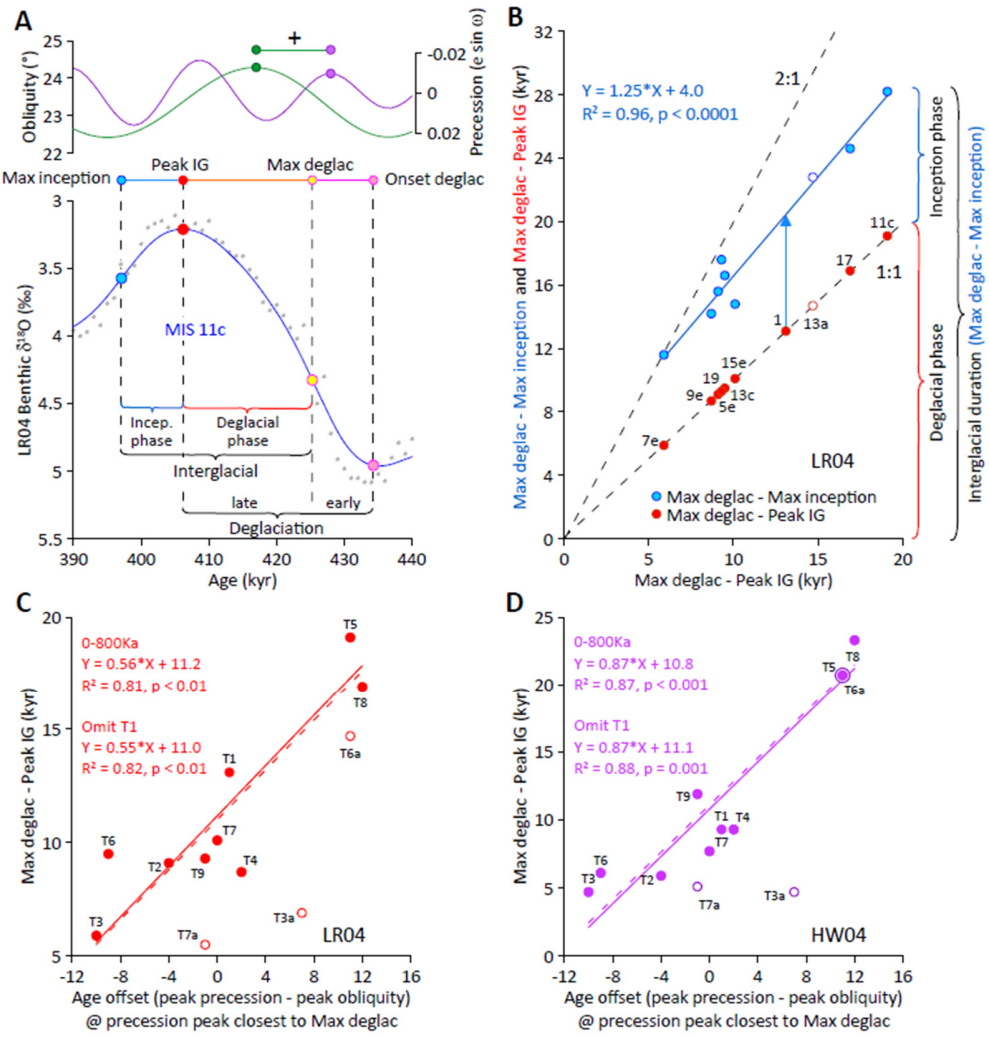

Fig. 2. Orbital phasing determines the duration of deglaciation. (A) Detail of interglacial anatomy for MIS 11c (associated with T5). Each interglacial is divided into a deglaciation phase (i.e. late deglaciation, between Max deglac and Peak IG) and a phase of glacial inception (between Peak IG and Max inception). Upper curves of precession and obliquity highlight offset between their respective peaks (positive in this case). (B) Correlation between Max deglac minus Max inception (interglacial duration) versus Max deglac minus Peak IG (deglacial phase; numbers are MIS). The inception phase is relatively invariant as compared with that of the deglacial phase, giving rise to increasingly asymmetric interglacials as their duration increases (see also Fig. 7A-C). The high value of R^2 implies that time to Max inception might be predicted for MIS 1 if we know the offset between Max deglac and Peak IG (blue arrow; see also Fig. 7D). (C, D) Correlation between Max deglac minus Peak IG and peak precession minus peak obliquity for LR04 and HW04. Dashed fits omit T1. Note that T3a, T6a/MIS13a and T7a (hollow symbols) are not included in the correlations (see discussion in Section 6). Equivalent correlations for other records are given in Figs. S3, S4.

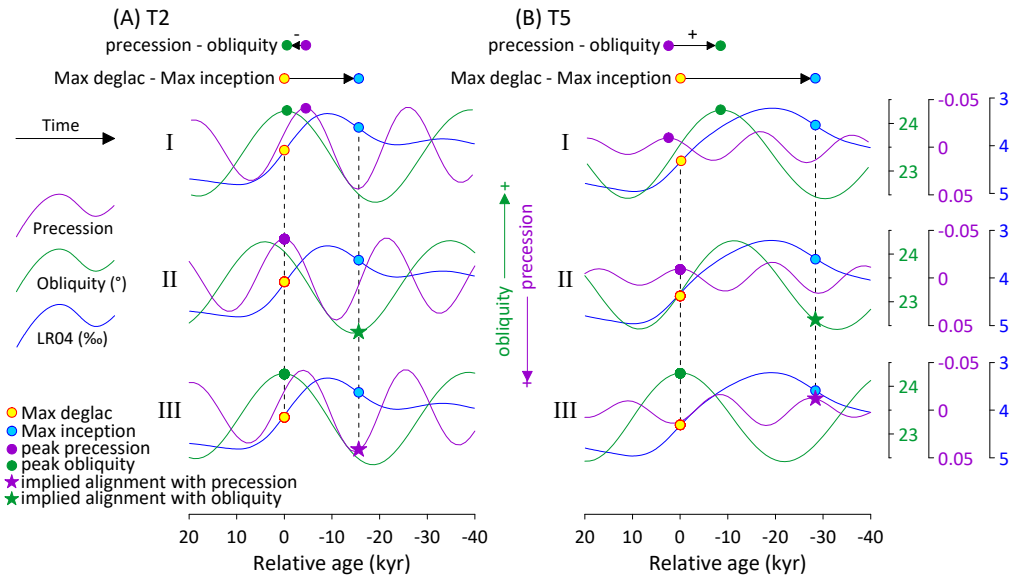

Fig. 3. Three scenarios for assessing which orbital parameter controls deglacial onset. Two deglacial intervals (A: T2 and B: T5) with contrasting orbital phasing illustrate the difference between Scenario I (original age models are accurate) versus Scenarios II and III, in which Max deglac is aligned with precession or obliquity respectively. Scenario II results in Max inception for both intervals being aligned consistently with respect to the phase of obliquity (which is expected when the correct starting parameter is chosen). In contrast, Scenario III results in misalignment of Max inception with respect to the phase of precession. See also Figure 4.

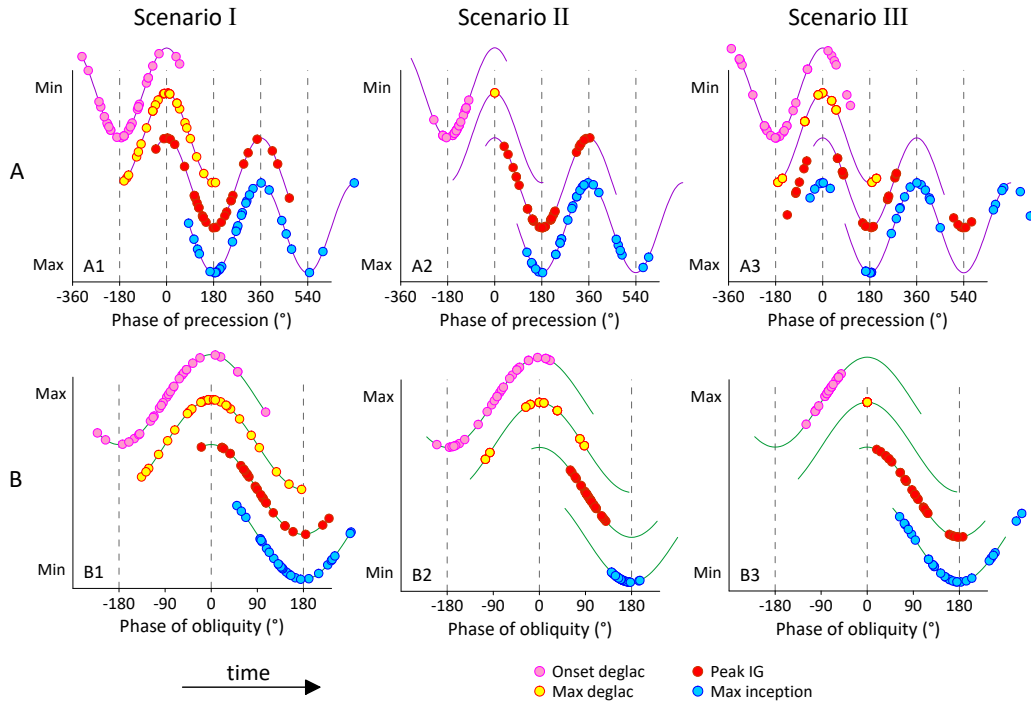

Fig. 4. Glacial inception aligns with obliquity when Max deglac is set to precession. Results for LR04_untuned, HW04 and U1476pmag from Scenarios I-III in Section 4. Each panel shows timing of Onset deglac, Max deglac, Peak IG and Max inception with respect to the phase of precession (row A) and obliquity (row B) for Terminations T2 to T12. In each case, zero phase is the closest precession/obliquity peak to Max deglac. Each individual point represents an individual termination/interglacial on one of the 3 timescales used. 10 terminations and 3 records gives a total of 30 points in each case (note some points are overlapping). Note in Scenario II (Max deglac set to peak precession; Part A2) much tighter clustering of Peak IG and Max inception with respect to obliquity (B2) as compared with Scenario I (B1). On the contrary, setting Max deglac to peak obliquity (Scenario III; B3) does not result in close alignment of Peak IG or Max inception with precession (A3). In addition, alignment between Onset deglac and Max deglac with respect to precession in Scenario III (A3) is significantly worse than in Scenario I (A1). See Figure S6 and Table S2 for more detail.

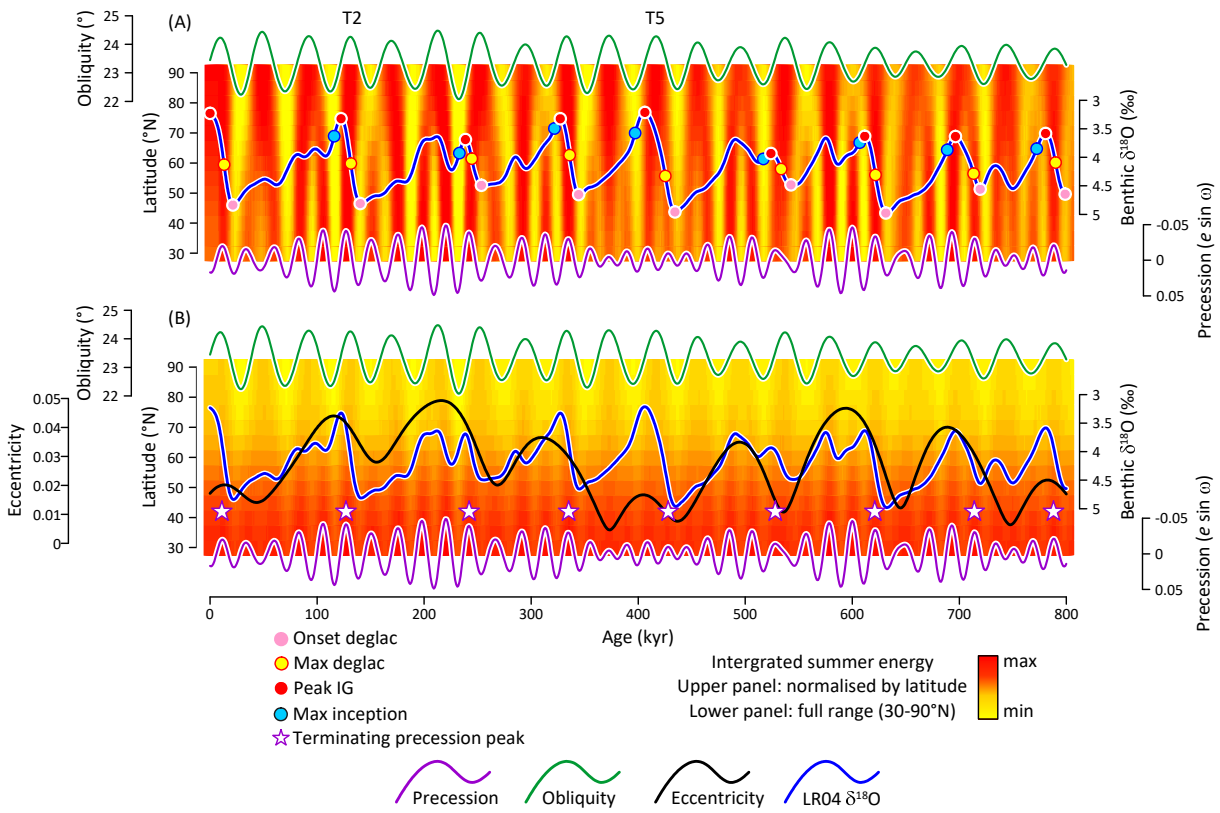

Fig. 5. Importance of latitude and inadequacy of a single insolation metric. (A) Upper and lowermost curves are obliquity and precession respectively (*72*), middle blue curve is the smoothed LR04 stack (*19*). Key events are indicated. Orange/yellow colors represent the integrated summer energy (*73*) normalized by each 5 degree band of latitude. Variability at lower latitudes is dominated by precession while higher latitudes (north of around 70°N) are dominated by obliquity. If deglaciation reflects the northward migration of the mean latitude (locus) of northern hemisphere land-based ice sheets, it can be appreciated why precession (at low latitudes) is more important for the earlier stages of deglaciation, while obliquity (at high latitudes) is more important for the end. No single insolation metric can be used to characterize this changing dependence. Note that for T5 (~420ka) precession and obliquity were out of phase, giving rise to a particularly long deglacial period as the initial stages of deglaciation gave way to the subsequent (lagged) development of full interglacial conditions. In contrast precession and obliquity were in phase during T2 (~130ka), resulting in a much shorter interval of deglaciation. (B) Same as (A) except that integrated summer energy is normalized across its entire range from 30 to 90°N. Ice sheets grow while eccentricity (black curve) decreases and obliquity is low. Purple stars are terminating precession peaks. Deglaciation may be triggered even if the amplitude of precession (a function of orbital eccentricity) is low (e.g. during T5) if ice sheets extend further to the south, where insolation is generally much higher than across more northerly latitudes.

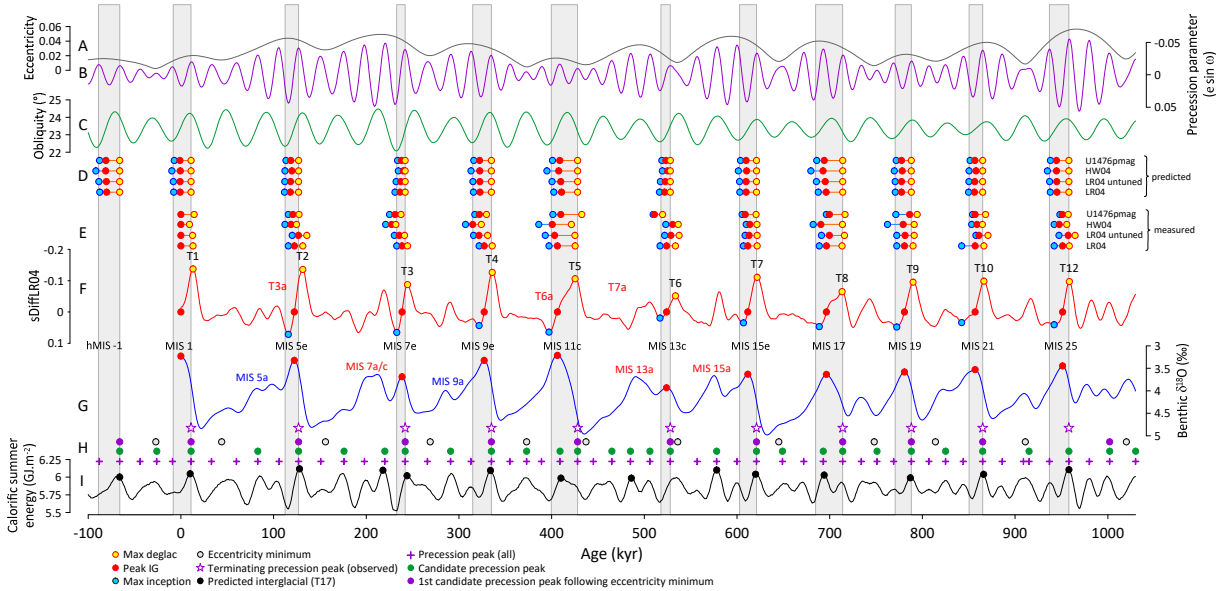

Fig. 6. Predicted occurrence and duration of glacial terminations and interglacials. (A-C) precession, obliquity and eccentricity (*72, 73*). (D) key events (Max deglac, Peak IG and Max inception) predicted from the relationships shown in Figs. 2C,D, S3,4. (E) same events measured directly from records of $\delta^{18}O$. (F) first differential of the LR04 stack (G). (H) Terminating precession peaks of the last 900kyr (purple stars and solid purple circles) are the subset of candidate peaks (green circles), which directly follow minima in eccentricity (grey circles). Candidate peaks are the subset of precession peaks (purple crosses) which begin when obliquity is increasing (or starts to increase within 2kyr of the turning point in precession (*16*)). (I) Integrated summer energy at 65°N (*73*) with black symbols indicating the predicted occurrence of interglacials based on the rule of ref (*10*) (T17). hMIS-1 is a hypothetical future interglacial. Vertical grey boxes indicate the predicted duration of interglacial periods (from Max deglac to Max inception) based on the average of predicted events in part (D).

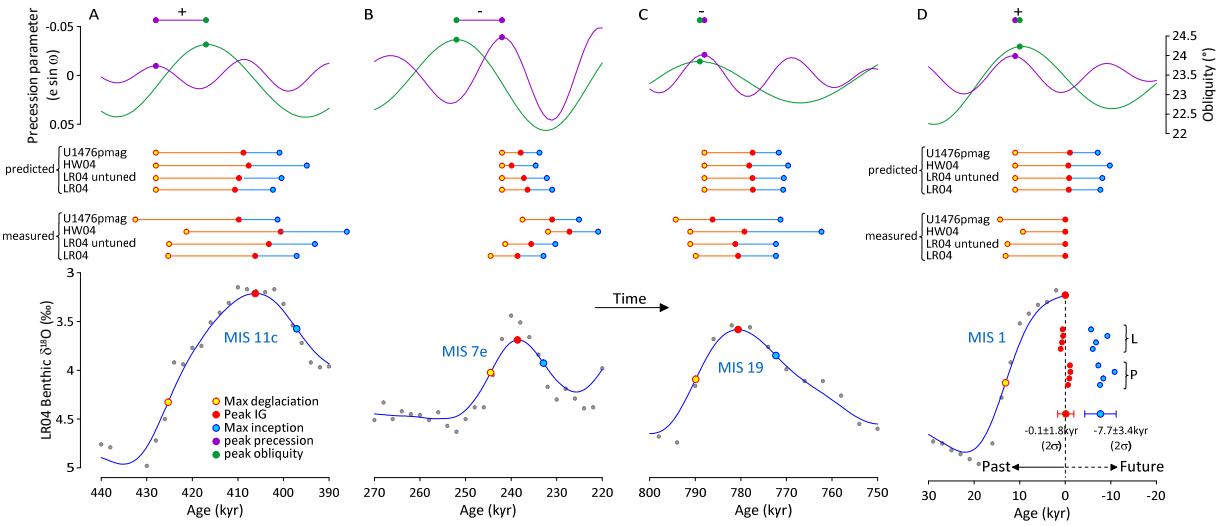

Fig. 7. Past and future predictions for the timing of Peak IG and glacial inception Note that time goes from left to right (A) Measured versus predicted occurrence of Max deglac, Peak IG and Max inception across T5 and MIS 11 (B, C) Same as (A) but for T3 (MIS 7e) and T9 (MIS 19) respectively. (D) Insolation variability across MIS 1 is similar to MIS 19. Isolated red and blue symbols are predictions of MIS 1 Peak IG and the next Max inception relative to Max deglac on LR04 (set L) and peak precession (set P) – see text.

Submitted Manuscript: Confidential
Template revised July 2024

Science
AAAS

Supplementary Materials for

Distinct roles for precession, obliquity and eccentricity in Pleistocene 100kyr glacial cycles

Stephen Barker, Lorraine E. Lisiecki, Gregor Knorr, Sophie Nuber, Polychronis C. Tzedakis.

Corresponding author: barkers3@cf.ac.uk

The PDF file includes:

Materials and Methods
Figs. S1 to S9
Tables S1 to S2

Materials and Methods

Treatment of benthic $\delta^{18}O$ records and stacks

We employ 3 independent records/stacks of benthic $\delta^{18}O$ on 4 independent timescales: (1) the LR04 stack (*19*) is based on 57 individual records of benthic $\delta^{18}O$ with global representation. The LR04 age model (below 135ka) was constructed by tuning to a simple ice volume model driven by June 21st insolation at 65°N. The uppermost 22kyr of the stack was tuned to a ^{14}C-dated record from North Atlantic site NA87-22 (*74*) while the interval 22-135ka was tuned to the Greenland ice core record via marine core MD95-2042 (*75*). (2) An untuned version of the LR04 stack (*14*) (LR04_untuned) was used for comparison to LR04. The age model for LR04_untuned was derived from radiometric (absolute) dates for the Brunhes/Matuyama and Matuyama/Gauss magnetic reversals. (3) the HW04 stack (*20, 21*) is based on 26 records of $\delta^{18}O$. The HW04 age model is based on radiometric dates for the Brunhes/Matuyama and Matuyama/Gauss magnetic reversals. (4) U1476pmag (*11*) is a single record of benthic $\delta^{18}O$ obtained from IODP Site U1476 in the western Indian Ocean. The age model for U1476pmag was derived from radiometric dating of 9 magnetic polarity reversals and magnetic excursions within the top 1.1Myr.

The LR04, LR04_untuned and U1476pmag records contain sub-orbital (millennial-scale) variability and require smoothing before the key points can be identified. Smoothing is implemented using a rectangular filter (running mean). The length of smoothing window affects the timing of key points (e.g. Peak IG and Max deglac; Fig. S1) and therefore the offsets between these points. However, a strong linear relationship between MaxDeglac-Peak IG versus precession-obliquity (as discussed in the main text) is observed for a wide range of smoothing window (Table S1) and, moreover, the predicted duration of MaxDeglac-Peak IG for Termination T1 (Fig. S7D) is relatively insensitive to the window length employed (variability is less than the difference between records; Table S1). We therefore utilize a window length of 9kyr, which is roughly halfway between the minimum value required to remove millennial-scale variability (7kyr (*76-78*)) and half of one precession period (~10.5kyr). HW04 is already smoothed and does not require additional smoothing before differentiating (Fig. S1).

After smoothing (Fig. S2), major interglacials are identified as local minima in $\delta^{18}O$ and designated as 'Peak IG'. The smoothed records are then differentiated to identify 'Max deglac' (peak rate of $\delta^{18}O$ decrease prior to Peak IG) and 'Max inception' (peak rate of $\delta^{18}O$ increase following Peak IG) for each major termination/interglacial. Onset deglac is defined as the point at which the rate of decreasing $\delta^{18}O$ reaches 10% of its peak value (which is the rate at Max deglac). This is to accommodate the effect of smoothing prior to differentiation (which effectively biases the turning point towards older ages; Fig. S3A). Increasing the threshold by ~10% decreases the offset between Onset deglac and Max deglac by ~1kyr with the effect being greatest for shorter deglacial periods such as T3, where the bias towards older ages is greatest.

Benthic foraminiferal $\delta^{18}O$ as an indicator of ice volume and deep ocean temperature

As with previous studies of this type (e.g. *2, 3, 5, 6, 10, 14*) our approach implicitly assumes that transitions in benthic $\delta^{18}O$ reflect changes in ice volume (at least in terms of their timing). However, foraminiferal $\delta^{18}O$ is also influenced by variations in deep ocean temperature and there is some evidence that systematic offsets may arise between the respective timing of changes in ice volume and deep ocean temperature across both glacial (*15*) and deglacial transitions (*79*). It is not possible here to account for such offsets but, if systematic in nature, they should have only a minor impact on our results. For example, estimates of sea level rise and mean ocean temperature across the last deglaciation suggest that the change in ice volume lagged mean ocean warming by a few kyr (*17*), leading to an offset of ~2kyr between the net change in benthic $\delta^{18}O$ (as measured, $\delta^{18}O_{foram}$) and the component driven specifically by ice volume ($\delta^{18}O_{ice}$) (*18*). Given that the total duration of deglaciation (from Onset deglac to Peak IG) varies from 14 to 28kyr we suggest that variations in the offset between $\delta^{18}O_{foram}$ and $\delta^{18}O_{ice}$ of a few kyr or less will not alter our conclusions.

Obviously it is important for future work to further elucidate the relative contributions of deep water temperature and ice volume on the record of benthic $\delta^{18}O$ and our study provides some testable targets for such work. For example, as noted, mean ocean warming across T1 preceded substantial sea level rise (*17*), leading to a lag of ~2kyr between the decrease in $\delta^{18}O$ recorded by benthic foraminifera and the component of that signal driven specifically by ice loss. On the other hand, the early warming is thought to have been a consequence of abrupt changes in ocean circulation and CO_2 release that were themselves a result of rising northern summer insolation (*17, 37, 50*). Thus, our finding that precession drives the initial stages of deglaciation (decreasing $\delta^{18}O$) remains logical even if some part of that decrease is driven by temperature. Further work should focus on constraining the temperature component of early deglaciation across a series of terminations to determine the extent of warming that might reflect changing precession versus that due to changes in ocean circulation.

A similar argument can be made for glacial inception. For example, reconstructions suggest that deep ocean cooling may have preceded ice sheet growth during the early stages of their development (*15*). Temperature of the

deep ocean is set in the high latitudes of both hemispheres, where obliquity dominates insolation variability. Thus the strong alignment we observe between Max inception and obliquity (Fig. 4) could in part reflect mean ocean cooling in addition to ice sheet growth. Furthermore, it is widely acknowledged that decreasing CO_2 plays a critical role in glacial inception (*29, 31, 71*). The concentration of atmospheric CO_2 on G-IG timescales is in large part determined by high latitude oceanic processes (*80*). In particular, deep ocean cooling during the early stages of the last glacial period (MIS 5e/d, which is equivalent to the point of Max inception following MIS 5e in our analysis; Fig. 1) may have been responsible for a significant decrease in CO_2 (*40, 81*). Thus the link between Max inception (maximum rate of $\delta^{18}O$ increase following Peak IG) and low to minimum obliquity (Fig. 4B2) might be viewed as the interplay between deep ocean cooling, decreasing CO_2 and ice sheet expansion.

Selecting the closest orbital peaks

After Max deglac is defined for each major termination, the closest peaks in precession and obliquity are identified (Fig. S2). The same set of precession peaks is identified for all stacks/records (Fig. S2D), even though age offsets between individual records may be as large as 18kyr; Fig. S3F). The same is true for peaks in obliquity, except for T3, where the peak selected for HW04 is one peak younger than that for all other records/stacks (Fig. S2E).

The fact that the same set of precession and obliquity peaks are selected for all records means that, in principle, we could use the correlation between Max deglac-Peak IG versus obliquity-precession at the closest obliquity peak to Max deglac, instead of Max deglac-Peak IG versus precession-obliquity at the closest precession peak (the relationship would be the same but negative). However, for particularly long terminations (e.g. T5 and T8) the limited range of obliquity-precession (±10.5kyr) would cause truncation of the correlation (Fig. S5). We therefore use Max deglac-Peak IG versus precession-obliquity at the closest precession peak in our calculations.

Phase relationships and statistical methods

Temporal offsets between key points in the curves of $\delta^{18}O$ are calculated directly from the various records on their original timescales (labelled 'measured' in Figs. 6, 7 and Table S2) or via the relationships given in Figures 2, S3, S4 (labelled 'predicted' in Figs. 6, 7 and Table S2). Temporal offsets are converted to phase offsets by assuming a constant period of 21kyr for precession and 41kyr for obliquity and are reported relative to the peak closest to Max deglac (defined as zero phase in each case).

Circular statistics shown in Fig. S6 and Table S2 were calculated using the CircStat toolbox for MATLAB developed by Berens (*82*). Below we summarize the various functions employed here:

Rayleigh test for a unimodal deviation from uniformity tests the null hypothesis (H_0) that the population is distributed uniformly around the circle. The approximate p-value under H_0 is computed as:

$$p = exp\left[\sqrt{(1 + 4N + 4(N^2 - r_n^2)} - (1 + 2N)\right]$$

where $r_n = r \cdot N$ (see below for definition of r). The lower the value of p, the greater the likelihood that H_0 can be rejected.

Mean angle ($\bar{\alpha}$). Individual directions are first transformed to unit vectors in the 2-D plane:

$$r_i = \begin{pmatrix} \cos \alpha_i \\ \sin \alpha_i \end{pmatrix}$$

The vectors r_i are then vector averaged:

$$\bar{r} = \frac{1}{N} \sum_i r_i$$

where $\bar{r}$ is the mean resultant vector. To yield the mean angular direction $\bar{\alpha}$ (rad), $\bar{r}$ is transformed using the four quadrant inverse tangent function (*82*).

Resultant vector length (r):

$$r = ||\bar{r}||$$

r varies between 0 and 1 with r closer to 1 if the data are more concentrated around the mean direction (i.e. more strongly aligned).

Standard deviation (s). The circular standard deviation (rad) is defined as:

$$s = \sqrt{-2 \ln (r)}$$

Linear statistics: All linear fits are performed using Reduced Major Axis (RMA) regression (which provides a more symmetric fit than ordinary least squares). RMA is typically used when errors exist in both X and Y, which is the case for the correlations between Max deglac minus Max inception and Max deglac minus Peak IG in Figure 2B (and Fig. S4). Furthermore, although the phase of precession relative to obliquity is known relatively accurately, we cannot assume a priori that the peak-to-peak offset is the correct parameter for assessing the phase relationship relevant for deglaciation. Therefore, and for consistency, we use RMA regression throughout our study.

How closely is Max deglac aligned with peak precession?

In this study we have made the case that the timing of deglaciation (in its earlier stages) is determined by precession and moreover that Max deglac should be aligned (approximately) with peak precession. We can assess the validity of this assertion using results across T1 (Fig. S9). Stern and Lisiecki (*83*) report ^{14}C-based age models for a set of regional δ^{18}O stacks, which we use to provide a set of ages for Max deglac. We find that in all regions Max deglac occurs ahead of peak precession (by 1.4 to 2.4kyr) with the global LR04 stack leading peak precession by 1.6kyr.

Notably, stacks from the Atlantic Ocean give the earliest ages for Max deglac and this is feasibly due in part to the effects of the millennial-scale HS1 event (~18-15ka) which involved major circulation changes within the Atlantic and marked the onset of T1. It has been argued that millennial-scale events such as HS1 can influence the shape and rapidity of glacial termination (*37*). Indeed, mean ocean temperature increased rapidly across HS1 (*84*), earlier than the decrease in ice volume (*17, 85*). This means that the initial decrease in benthic δ^{18}O across T1 was primarily driven by temperature, resulting in an effective lag of ~2kyr between the net rise in benthic δ^{18}O and the specific component associated with decreasing ice volume (*18*) (which is similar to the aforementioned offset between Max deglac and peak precession).

Events equivalent to HS1 occurred during the early phases of all terminations throughout the past 1Ma (*11, 55*) and we might therefore expect a systematic lead of Max deglac ahead of peak precession, reflecting early warming of the mean ocean ahead of significant ice sheet decay. In fact the systematic nature of such an effect might explain why the temporal offset between Onset deglac and Max deglac is so consistent from one termination to the next (Fig. 1). Further investigation of these processes is clearly needed but here we conclude that while Max deglac and peak precession might be misaligned due to millennial-scale feedbacks within the climate system, the misalignment (by analogy with T1) should be of the order 2.5kyr or less.

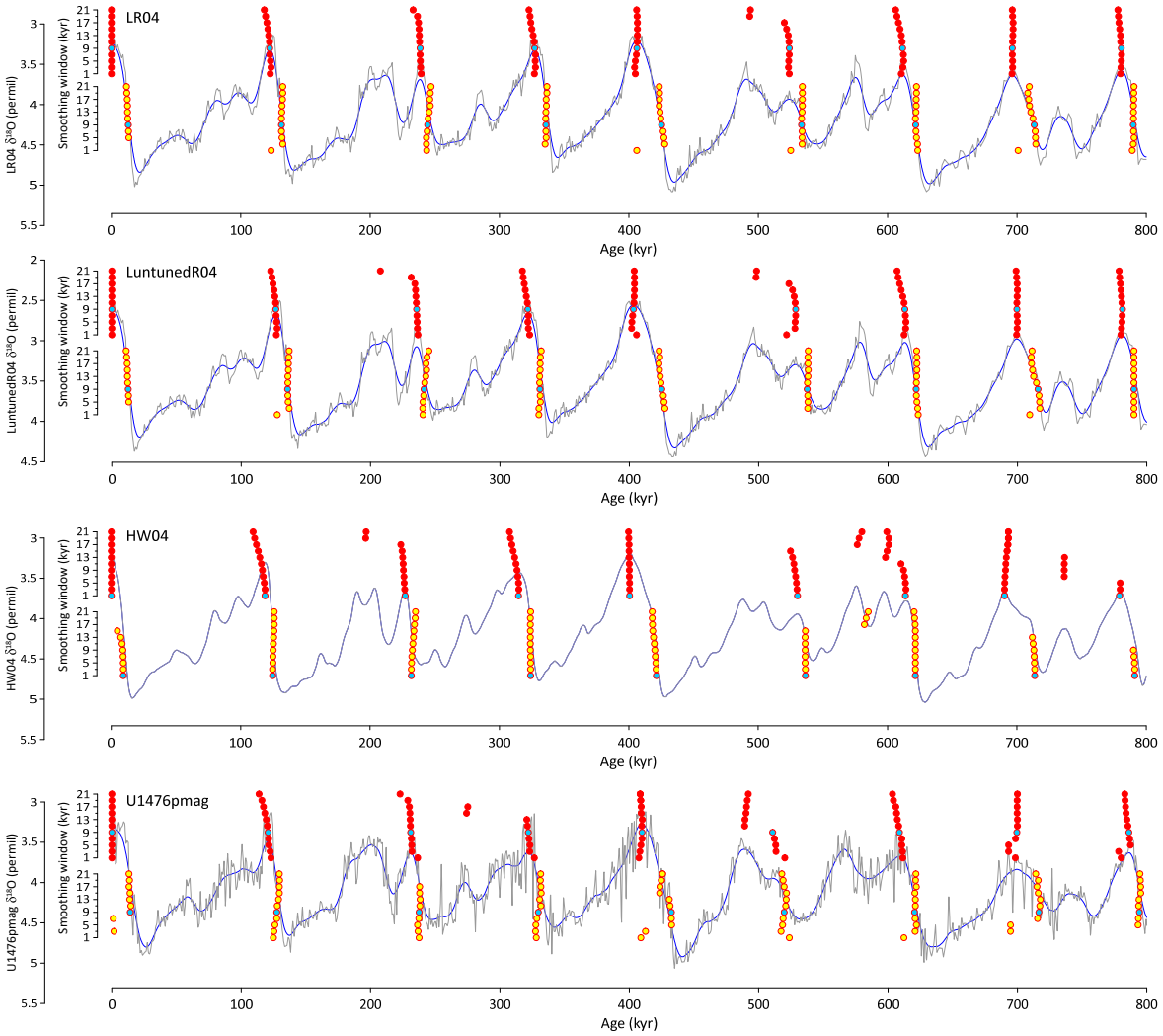

Fig. S1. Effect of smoothing window length on the timing of Peak IG and Max deglac. Red and yellow symbols represent Peak IG and Max deglac (respectively) for various smoothing windows (1:2:21kyr) of each curve. Blue symbols represent window length adopted in this study (9kyr for LR04, LR04_untuned and U1476pmag, 1kyr for HW04). Blue curve in each panel is the relevant record smoothed according to the specified window length. Grey curve is raw stack/record (HW04 is already smoothed).

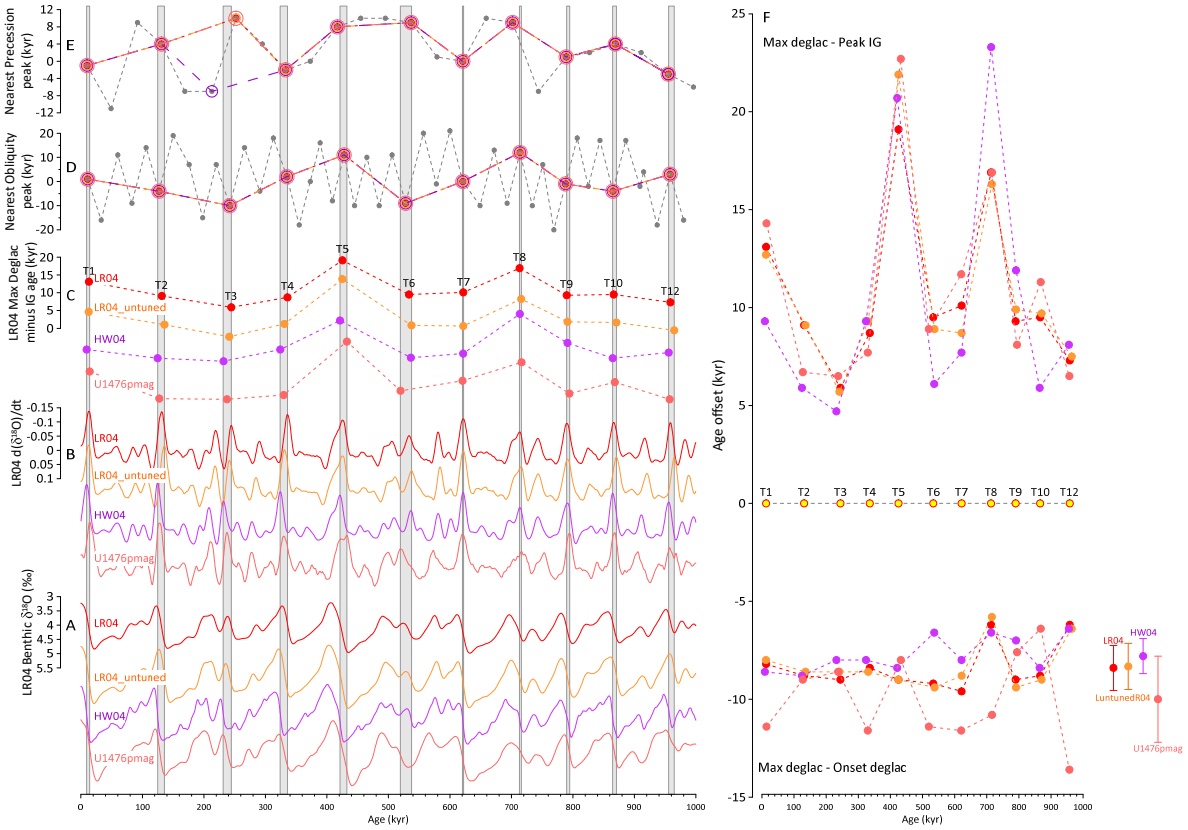

Fig. S2. Summary of results for 3 records/stacks of benthic $\delta^{18}O$ on 4 independent age models. (A) Smoothed records/stacks of benthic $\delta^{18}O$ (B) First differential of $\delta^{18}O$ (C) Max deglac minus Peak IG reveals similar variations among the 4 records/timescales (D) Grey symbols show the offset between each precession peak over past 1Myr and its nearest obliquity neighbour. Coloured symbols highlight those precession peaks that are closest to each Max deglac (the same precession peaks are selected for all records/timescales). Note the similar relationship between deglacial duration (C; Max deglac – Peak IG) and precession-obliquity (in D) as observed for the LR04 stack and shown in Fig. 1. See also Figs. 2, S3, S4. (E) Same as (D) but for obliquity. The same obliquity peaks are selected for each record except HW04 for T3, which is closer to a later obliquity peak than the other records. (F) The duration between Onset deglac and Max deglac is relatively invariant as compared with Max deglac – Peak IG.

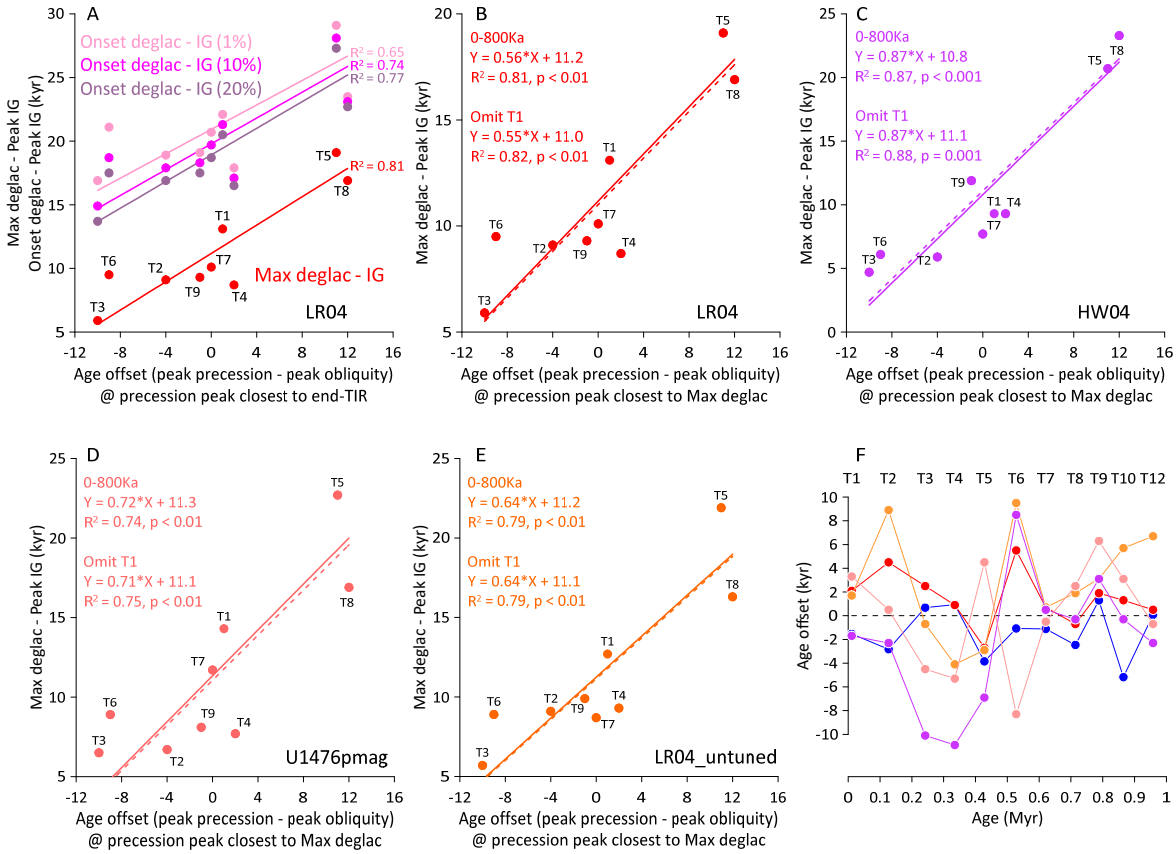

Fig. S3. Correlations between deglacial duration and the phasing of precession versus obliquity. (A) Comparison of Onset deglaciation minus Peak IG age (i.e. 'full width' of deglaciation) beginning at 1, 10 and 20% of max rate of deglaciation (see text) with Max deglac minus Peak IG age. The relatively constant offset between Onset deglac minus Peak IG and Max deglac minus Peak IG (see also Fig. 1) reflects the fact that most of the variability in the duration of deglacials involves the latter half of deglaciation (i.e. between Max deglac and Peak IG). (B-E) Max deglac minus Peak IG age versus precession minus obliquity for 3 records/stacks of benthic $\delta^{18}O$ on 4 independent age models. (F) Age offsets between Max deglac and peak precession for each record over past 1Myr. Age offsets between individual age models may be up to 18kyr but the same precession peaks are selected for each termination for all records (see also Fig. S2).

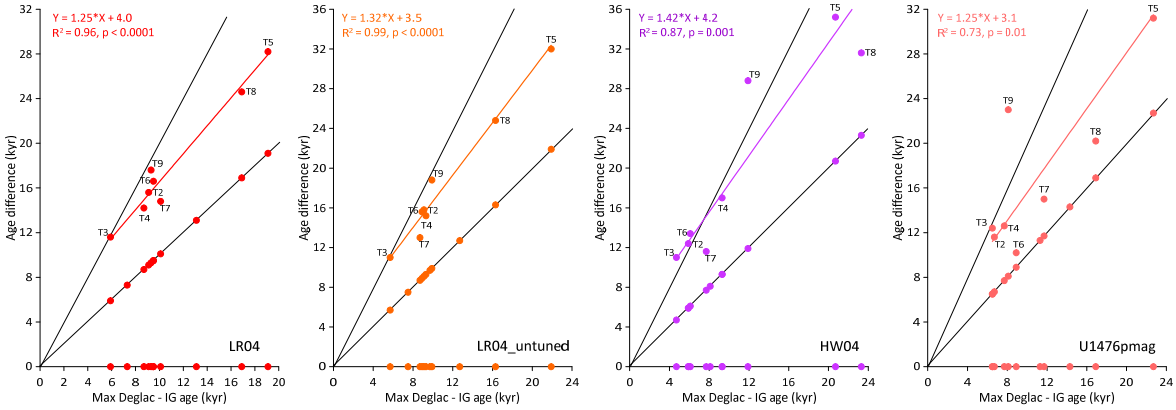

204

205 **Fig. S4. Variations in interglacial duration are dominated by the deglacial interval.**
206 Correlations between Max deglac minus Max inception versus Max deglac minus Peak IG for
207 each of the benthic $\delta^{18}O$ records/stacks analysed in this study (see also Fig. 2).
208

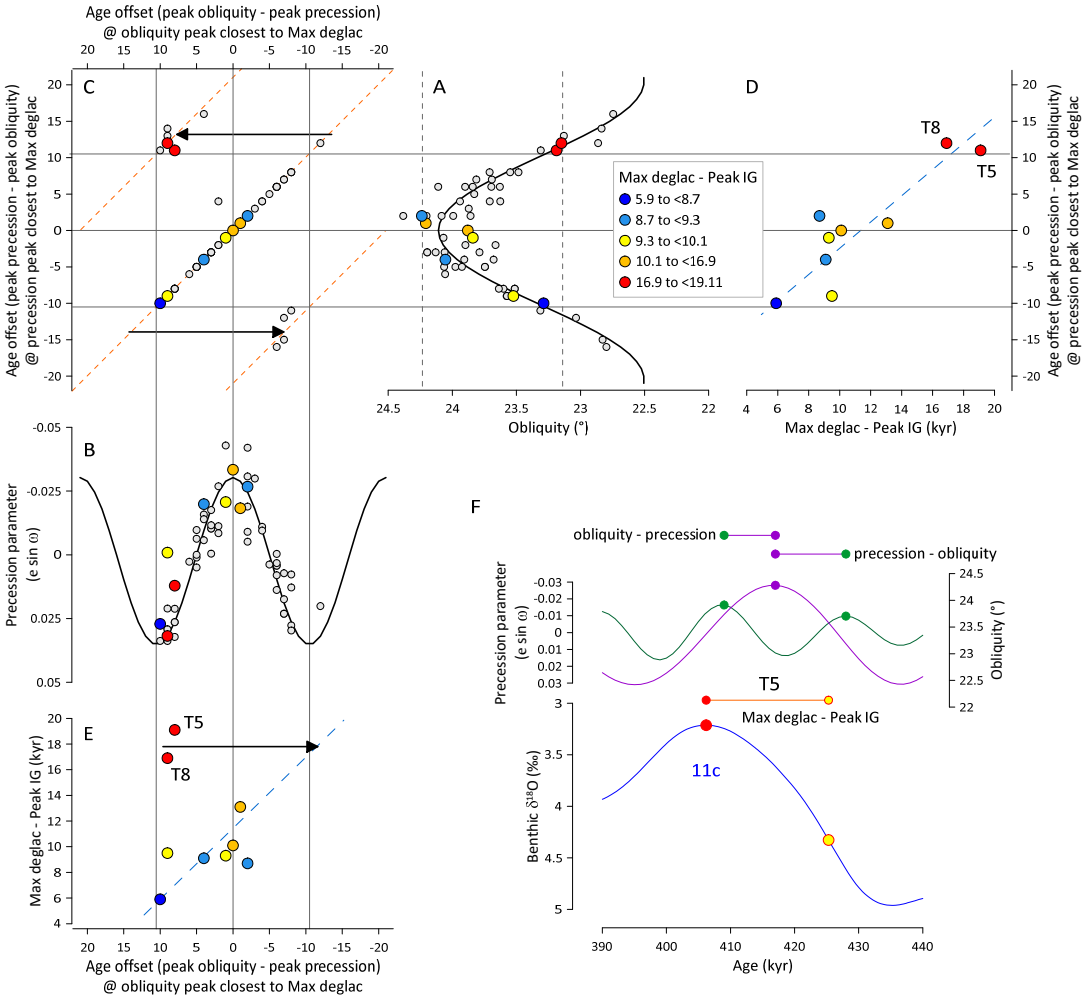

Fig. S5. Precession-minus-obliquity versus obliquity-minus-precession. (A) Value of obliquity at the precession peaks closest to all deglacial transitions in LR04 over the past 2Myr versus the peak-to-peak offset between precession and obliquity (i.e. precession-obliquity). Coloured symbols (coloured according to the respective offset between Max deglac and Peak IG) correspond to major terminations of the past 0.8Myr. (B) Same as (A) but this time symbols represent value of precession at the obliquity peaks closest to all deglacial transitions versus the peak-to-peak offset between obliquity and precession (i.e. obliquity-precession). Note reduced range of obliquity-precession in (B) compared with precession-obliquity in (A) due to the fact that the closest precession peak can be no further than 10.5kyr from a given peak in obliquity while the closest obliquity peak can be up to 20.5kyr from a given peak in precession. (C) This results in an incorrect obliquity-precession offset being assigned to particularly long deglaciations (e.g. T5 in part (F)) where the nearest precession peak to the closest obliquity peak to Max deglac is not the same as the closest precession peak to Max deglac. The resulting correlation between Max deglac-Peak IG and obliquity-precession (E) is truncated when compared with that between Max deglac-Peak IG and precession-obliquity (D).

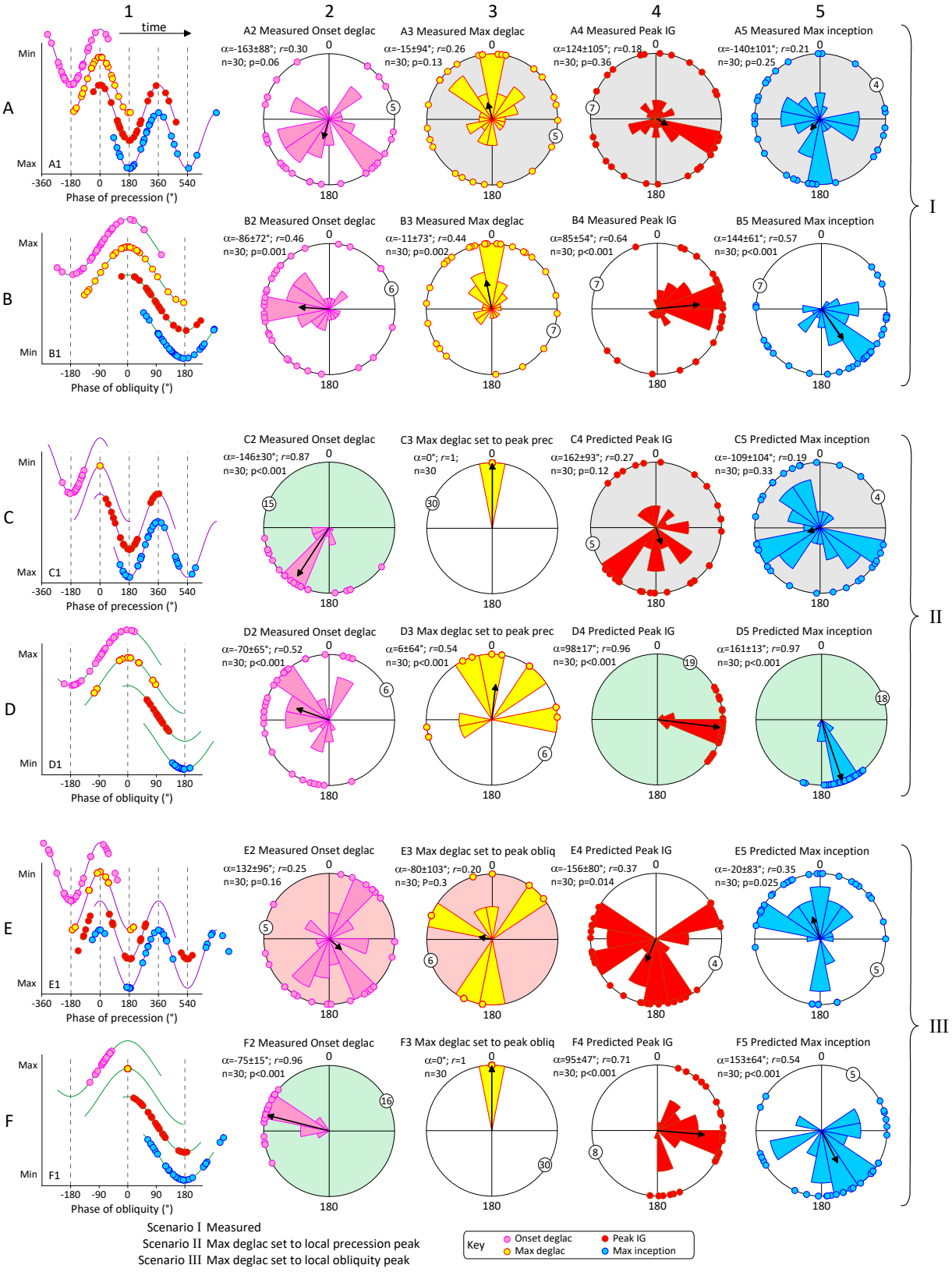
1
2
3
4
5
time
A
B
C
D
E
F
Min
Max
A1
B1
C1
D1
E1
F1
-360 -180 0 180 360 540
Phase of precession (°)
-180 -90 0 90 180
Phase of obliquity (°)
A2 Measured Onset deglac
α=-163±88°; r=0.30
n=30; p=0.06
A3 Measured Max deglac
α=-15±94°; r=0.26
n=30; p=0.13
A4 Measured Peak IG
α=124±105°; r=0.18
n=30; p=0.36
A5 Measured Max inception
α=-140±101°; r=0.21
n=30; p=0.25
B2 Measured Onset deglac
α=-86±72°; r=0.46
n=30; p=0.001
B3 Measured Max deglac
α=-11±73°; r=0.44
n=30; p=0.002
B4 Measured Peak IG
α=85±54°; r=0.64
n=30; p<0.001
B5 Measured Max inception
α=144±61°; r=0.57
n=30; p<0.001
C2 Measured Onset deglac
α=-146±30°; r=0.87
n=30; p<0.001
C3 Max deglac set to peak prec
α=0°; r=1;
n=30
C4 Predicted Peak IG
α=162±93°; r=0.27
n=30; p=0.12
C5 Predicted Max inception
α=-109±104°; r=0.19
n=30; p=0.33
D2 Measured Onset deglac
α=-70±65°; r=0.52
n=30; p<0.001
D3 Max deglac set to peak prec
α=6±64°; r=0.54
n=30; p<0.001
D4 Predicted Peak IG
α=98±17°; r=0.96
n=30; p<0.001
D5 Predicted Max inception
α=161±13°; r=0.97
n=30; p<0.001
E2 Measured Onset deglac
α=132±96°; r=0.25
n=30; p=0.16
E3 Max deglac set to peak obliq
α=-80±103°; r=0.20
n=30; P=0.3
E4 Predicted Peak IG
α=-156±80°; r=0.37
n=30; p=0.014
E5 Predicted Max inception
α=-20±83°; r=0.35
n=30; p=0.025
F2 Measured Onset deglac
α=-75±15°; r=0.96
n=30; p<0.001
F3 Max deglac set to peak obliq
α=0°; r=1
n=30
F4 Predicted Peak IG
α=95±47°; r=0.71
n=30; p<0.001
F5 Predicted Max inception
α=153±64°; r=0.54
n=30; p<0.001
I
II
III
Scenario I Measured
Scenario II Max deglac set to local precession peak
Scenario III Max deglac set to local obliquity peak
Key
Onset deglac
Max deglac
Peak IG
Max inception

224

Fig. S6. Precession determines the onset of deglaciation. Results for LR04_untuned, HW04 and U1476pmag from Scenarios I-III in Section 4 (see also Table S2). Column (1) (repeated from Fig. 4) timing of Onset deglac, Max deglac, Peak IG and Max inception with respect to the phase of precession and obliquity for Terminations T2 to T12. In each case, zero phase is the closest precession/obliquity peak to Max deglac. Columns (2-5) represent the same results using rose diagrams to illustrate the relative phasing for individual records. In each case α is the mean direction $\pm 1\sigma$ for all events, r is length of the mean resultant vector ($r \rightarrow 1$ as data converge; see Methods). Black arrow is the mean resultant vector (angle = α, length = r * radial axis). Circled number is length of radial axis. In Scenario I (rows A, B) each event is derived directly from the published records on their respective age models. In Scenario II (rows C, D) Max deglac is set to the nearest precession peak (C3). Offsets from Onset deglac to Max deglac are measured (C2, D2) while Max deglac to Peak IG (C4, D4) and Max inception (C5, D5) are predicted from relationships in Figs 2, S3. In Scenario III (rows E, F) Max deglac is set to the nearest obliquity peak (F3). Grey shading indicates $p>0.1$, pink shading indicates $p>0.1$ with respect to Scenario I (i.e. alignment is significantly worse), green shading indicates $r > 0.8$ and $r > 0.1$ with respect to Scenario I (i.e. alignment is significantly stronger).

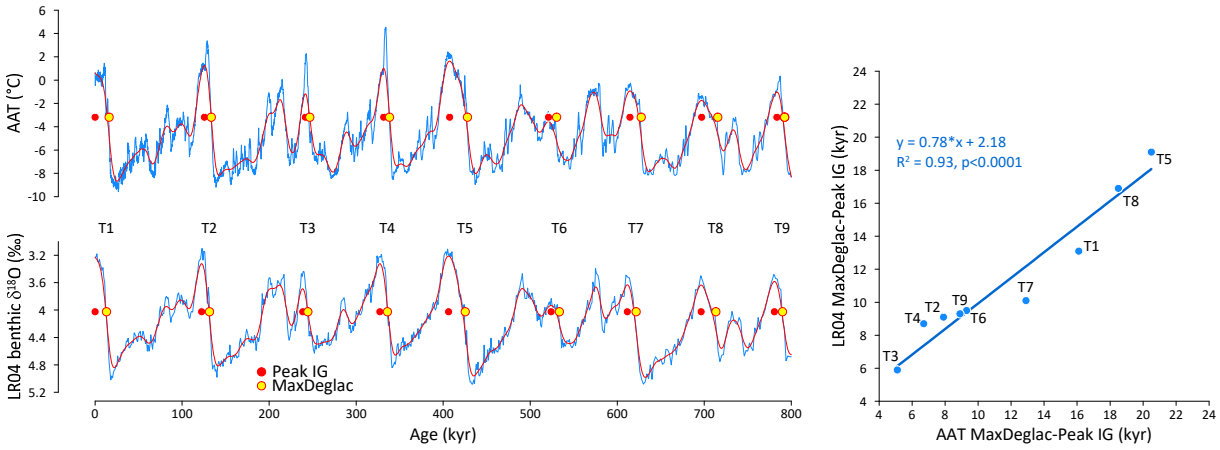

Fig. S7. Morphological similarity of Antarctic temperature and LR04 benthic $\delta^{18}O$ stack. Close agreement between the shape of AAT (in this case the stacked record of Parrenin et al., (*44*) on the AICC2012 timescale (*86, 87*)) and LR04 implies a common control across deglaciation. Pre-treatment (i.e. smoothing and differentiating) of AAT was identical to that described for LR04 in Methods.

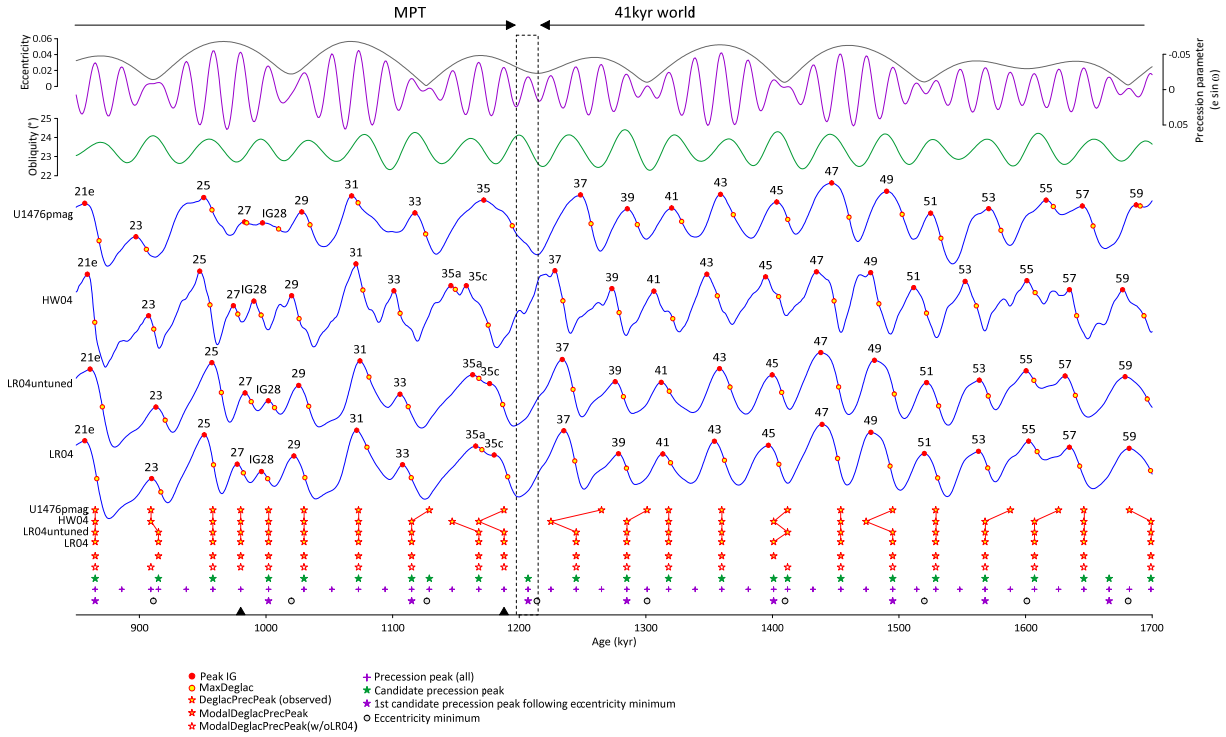

Fig. S8. Deglaciations of the 41kyr world and MPT. Prior to the MPT deglacial transitions were more closely aligned with candidate precession peaks (i.e. those that commenced while obliquity was increasing) than with non-candidate peaks, with almost all candidate peaks being associated with a deglacial event. This resulted in glacial periods being roughly equal in length to the period of obliquity, and implies no (significant) influence of eccentricity on glacial periods prior to the MPT. A similar situation is observed during the MPT except that deglacial events were also (occasionally) aligned with non-candidate precession peaks (indicated by black triangles). The first of these events (the deglaciation leading into MIS 35c) followed the first instance of a rise in obliquity not being associated with deglaciation (dotted rectangle). As noted previously (*11*) the subsequent fall in obliquity was the only instance during the past 1.7Myr when a minimum in obliquity was not associated with the onset or continuation of significant ice rafting across the North Atlantic. The interval highlighted by the dotted rectangle can therefore be considered as the definitive end of the 41kyr world. 'DeglacPrecPeak (observed)' = nearest precession peak to MaxDeglac for each stack/record of benthic $\delta^{18}O$; 'ModalDeglacPrecPeak' = average (modal) precession peak for the various records on 4 independent age models (where no mode exists the peak closest to the mean age is selected); 'ModalDeglacPrecPeak(w/oLR04)' = same, but not including LR04.

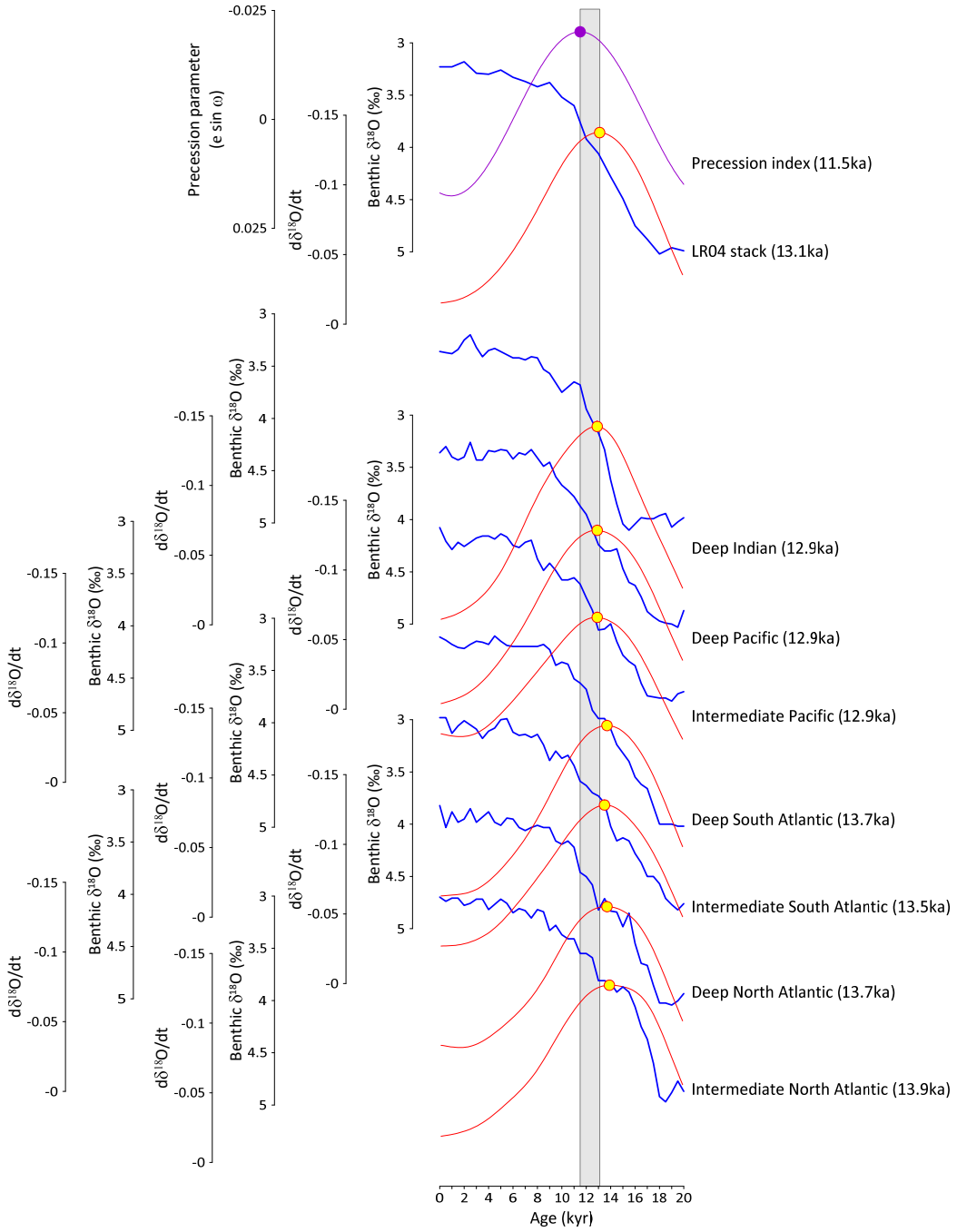

Fig. S9. Timing of Max deglaciation across Termination 1 (T1) versus peak (minimum) precession. Uppermost curve is precession parameter with peak highlighted by purple symbol. Also plotted at top is the LR04 benthic $\delta^{18}O$ stack along with its rate of change (Max deglac is highlighted by yellow symbol). According to the LR04 age model Max deglac occurred ~13.1ka, 1.6kyr before the peak in precession. Other curves show results for regional benthic $\delta^{18}O$ stacks as derived by Stern and Lisiecki (*83*). Grey box spans age estimates for peak precession and LR04 stack. These results suggest that Max deglac can be assumed to align with a minimum in precession with an uncertainty of ~2.5kyr.

						Termination 1			Termination 5		
							Calculated (predicted)			Calculated (predicted)	
	Smooth (kyr)	A	B	n	R^2	Prec-Obl (kyr)	MaxDeglac-Peak IG (kyr)	1σ	Prec-Obl (kyr)	MaxDeglac-Peak IG (kyr)	1σ
LR04	7	0.632	11.17	8	0.78	2	12.4		11	18.1	
	8	0.597	11.12	8	0.80	2	12.3		11	17.7	
	9	0.550	11.01	8	0.81	2	12.1		11	17.1	
	10	0.513	11.01	8	0.80	2	12.0		11	16.7	
	11	0.473	11.04	8	0.80	2	12.0		11	16.2	
	12	0.430	11.17	8	0.78	2	12.0		11	15.9	
							12.2	0.2		16.9	0.9
Luntuned04	7	0.723	11.41	8	0.77	2	12.9		11	19.4	
	8	0.693	11.34	8	0.78	2	12.7		11	19.0	
	9	0.641	11.14	8	0.79	2	12.4		11	18.2	
	10	0.598	11.13	8	0.79	2	12.3		11	17.7	
	11	0.555	11.26	8	0.77	2	12.4		11	17.4	
	12	0.504	11.41	8	0.74	2	12.4		11	17.0	
							12.5	0.2		18.1	0.9
HW04	1	0.865	11.09	8	0.88	2	12.8		11	20.6	
	2	0.855	10.94	8	0.87	2	12.7		11	20.3	
	3	0.853	11.02	8	0.87	2	12.7		11	20.4	
	4	0.834	11.10	8	0.87	2	12.8		11	20.3	
	5	0.810	11.20	8	0.87	2	12.8		11	20.1	
	6	0.783	11.33	8	0.87	2	12.9		11	19.9	
							12.8	0.1		20.3	0.2
U1476pmag	7	0.772	10.08	8	0.77	2	11.6		11	18.6	
	8	0.747	10.71	8	0.79	2	12.2		11	18.9	
	9	0.709	11.06	8	0.75	2	12.5		11	18.9	
	10	0.638	11.47	8	0.74	2	12.7		11	18.5	
	11	0.701	11.27	7	0.83	2	12.7		11	19.0	
	12	0.704	11.29	7	0.79	2	12.7		11	19.0	
							12.4	0.4		18.8	0.2

Table S1. Effect of smoothing window (applied to benthic $\delta^{18}O$ records/stacks before differentiating) on RMA linear fits of MaxDeglac-Peak IG versus precession-obliquity (MaxDeglac-Peak IG = Ax+B, where x = precession-obliquity) (Fig. S3). Fits are based on T2-9 (i.e. excluding T1). The difference in calculated MaxDeglac-Peak IG is minimal for low peak-to-peak offsets (e.g. T1), rising to several hundred years for larger offsets, depending on the record employed. The smoothing window used for the final calculations in each case is indicated by green shading.

Scenario I: Measured

1.1. Relative to local precession peak (Fig. S6A)

	Onset Deglac					Max Deglac					Peak IG					Max inception				
	n	p value	*r*	Angle	1σ	n	p value	*r*	Angle	1σ	n	p value	*r*	Angle	1σ	n	p value	*r*	Angle	1σ
LR04	10	0.01	0.68	-169	51	10	0.00	0.79	-24	39	10	0.04	0.56	99	62	10	0.16	0.43	-153	75
LuntunedR04	10	0.44	0.29	-180	90	10	0.41	0.30	-49	89	10	0.41	0.30	67	89	10	0.44	0.29	-179	90
HW04	10	0.56	0.24	-108	96	10	0.66	0.21	24	102	10	0.37	0.32	121	87	10	0.83	0.14	171	114
U1476pmag	10	0.08	0.50	-177	67	10	0.27	0.37	-10	81	10	0.47	0.28	-160	91	10	0.15	0.43	-99	74
All events	**40**	**0.00**	**0.40**	**-166**	**78**	**40**	**0.00**	**0.39**	**-20**	**78**	**40**	**0.05**	**0.27**	**112**	**92**	**40**	**0.06**	**0.27**	**-145**	**93**
All events w/o LR04	**30**	**0.06**	**0.30**	**-163**	**88**	**30**	**0.13**	**0.26**	**-15**	**94**	**30**	**0.36**	**0.18**	**124**	**105**	**30**	**0.25**	**0.21**	**-140**	**101**

1.2. Relative to local obliquity peak (Fig. S6B)

	Onset Deglac					Max Deglac					Peak IG					Max inception				
	n	p value	*r*	Angle	1σ	n	p value	*r*	Angle	1σ	n	p value	*r*	Angle	1σ	n	p value	*r*	Angle	1σ
LR04	10	0.00	0.77	-86	41	10	0.00	0.72	-11	46	10	0.00	0.89	80	28	10	0.00	0.80	146	38
LuntunedR04	10	0.01	0.68	-105	50	10	0.02	0.61	-28	57	10	0.00	0.73	70	46	10	0.00	0.75	127	44
HW04	10	0.05	0.54	-61	63	10	0.07	0.51	5	67	10	0.00	0.71	103	48	10	0.08	0.50	177	68
U1476pmag	10	0.59	0.23	-92	98	10	0.54	0.25	-2	95	10	0.05	0.54	82	64	10	0.03	0.58	139	60
All events	**40**	**0.00**	**0.54**	**-86**	**64**	**40**	**0.00**	**0.51**	**-11**	**66**	**40**	**0.00**	**0.70**	**83**	**48**	**40**	**0.00**	**0.63**	**145**	**55**
All events w/o LR04	**30**	**0.00**	**0.46**	**-86**	**72**	**30**	**0.00**	**0.44**	**-11**	**73**	**30**	**0.00**	**0.64**	**85**	**54**	**30**	**0.00**	**0.57**	**144**	**61**

Scenario II: Max deglac set to closest precession peak

2.1. Relative to local precession peak

2.1.1. Measured offsets

	Onset Deglac					Max Deglac					Peak IG					Max inception				
	n	p value	*r*	Angle	1σ	n	p value	*r*	Angle	1σ	n	p value	*r*	Angle	1σ	n	p value	*r*	Angle	1σ
LR04	10	0.00	0.94	-145	20			1	0		10	0.04	0.57	156	61	10	0.30	0.35	-93	83
LuntunedR04	10	0.00	0.94	-144	20			1	0		10	0.02	0.61	148	57	10	0.04	0.56	-110	62
HW04	10	0.00	0.97	-131	14			1	0		10	0.02	0.61	109	57	10	0.00	0.79	-149	40
U1476pmag	10	0.00	0.81	-169	38			1	0		10	0.04	0.55	139	63	10	0.08	0.50	-152	67
All events	**40**	**0.00**	**0.89**	**-146**	**28**			**1**	**0**		**40**	**0.00**	**0.56**	**138**	**62**	**40**	**0.00**	**0.50**	**-131**	**67**
All events w/o LR04	**30**	**0.00**	**0.87**	**-146**	**30**			**1**	**0**		**30**	**0.00**	**0.56**	**132**	**61**	**30**	**0.00**	**0.58**	**-138**	**59**

2.1.2. Measured/Predicted offsets (Fig. S6C)

LR04	"	"	"	"	"			"	"		10	0.11	0.47	-177	70	10	0.42	0.30	-75	89
LuntunedR04	"	"	"	"	"			"	"		10	0.27	0.37	176	81	10	0.66	0.21	-100	102
HW04	"	"	"	"	"			"	"		10	0.68	0.20	126	103	10	0.70	0.19	-97	104
U1476pmag	"	"	"	"	"			"	"		10	0.47	0.28	167	91	10	0.69	0.20	-130	103
All events	"	"	"	"	"			"	"		**40**	**0.02**	**0.31**	**170**	**88**	**40**	**0.17**	**0.21**	**-97**	**101**
All events w/o LR04	"	"	"	"	"			"	"		**30**	**0.12**	**0.27**	**162**	**93**	**30**	**0.33**	**0.19**	**-109**	**104**

2.2. Relative to local obliquity peak

2.2.1. Measured offsets

	Onset Deglac					Max Deglac					Peak IG					Max inception				
	n	p value	*r*	Angle	1σ	n	p value	*r*	Angle	1σ	n	p value	*r*	Angle	1σ	n	p value	*r*	Angle	1σ
LR04	10	0.02	0.60	-69	58	10	0.05	0.54	6	64	10	0.00	0.78	92	40	10	0.00	0.72	158	46
LuntunedR04	10	0.02	0.60	-69	58	10	0.05	0.54	6	64	10	0.00	0.80	94	39	10	0.00	0.83	155	35
HW04	10	0.05	0.55	-62	63	10	0.05	0.54	6	64	10	0.00	0.89	91	27	10	0.01	0.68	161	51
U1476pmag	10	0.15	0.44	-81	73	10	0.05	0.54	6	64	10	0.00	0.76	94	43	10	0.01	0.66	143	52
All events	**40**	**0.00**	**0.54**	**-70**	**63**	**40**	**0.00**	**0.54**	**6**	**64**	**40**	**0.00**	**0.81**	**93**	**37**	**40**	**0.00**	**0.72**	**154**	**47**
All events w/o LR04	**30**	**0.00**	**0.52**	**-70**	**65**	**30**	**0.00**	**0.54**	**6**	**64**	**30**	**0.00**	**0.82**	**93**	**37**	**30**	**0.00**	**0.72**	**153**	**47**

2.2.2. Measured/Predicted offsets (Fig. S6D)

LR04	"	"	"	"	"	"	"	"	"	"	10	0.00	0.89	99	27	10	0.00	0.95	158	19
LuntunedR04	"	"	"	"	"	"	"	"	"	"	10	0.00	0.93	99	22	10	0.00	0.99	161	10
HW04	"	"	"	"	"	"	"	"	"	"	10	0.00	0.99	95	8	10	0.00	0.97	171	15
U1476pmag	"	"	"	"	"	"	"	"	"	"	10	0.00	0.96	99	17	10	0.00	0.99	151	6
All events	"	"	"	"	"	"	"	"	"	"	**40**	**0.00**	**0.94**	**98**	**20**	**40**	**0.00**	**0.97**	**160**	**15**
All events w/o LR04	"	"	"	"	"	"	"	"	"	"	**30**	**0.00**	**0.96**	**98**	**17**	**30**	**0.00**	**0.97**	**161**	**13**

Scenario III: Max deglac set to closest obliquity peak

3.1. Relative to local precession peak

3.1.1. Measured offsets

	Onset Deglac					Max Deglac					Peak IG					Max inception				
	n	p value	*r*	Angle	1σ	n	p value	*r*	Angle	1σ	n	p value	*r*	Angle	1σ	n	p value	*r*	Angle	1σ
LR04	10	0.62	0.22	119	99	10	0.68	0.20	-80	103	10	0.07	0.51	143	66	10	0.09	0.49	-68	69
LuntunedR04	10	0.61	0.23	124	99	10	0.68	0.20	-80	103	10	0.13	0.46	152	72	10	0.62	0.22	-65	99
HW04	10	0.65	0.21	136	101	10	0.68	0.20	-80	103	10	0.40	0.31	-152	88	10	0.39	0.31	78	87
U1476pmag	10	0.40	0.31	135	88	10	0.68	0.20	-80	103	10	0.26	0.37	152	81	10	0.97	0.05	-147	140
All events	**40**	**0.10**	**0.24**	**129**	**97**	**40**	**0.20**	**0.20**	**-80**	**103**	**40**	**0.00**	**0.38**	**159**	**80**	**40**	**0.56**	**0.12**	**-51**	**118**
All events w/o LR04	**30**	**0.16**	**0.25**	**132**	**96**	**30**	**0.30**	**0.20**	**-80**	**103**	**30**	**0.03**	**0.34**	**166**	**84**	**30**	**0.94**	**0.05**	**33**	**142**

3.1.2. Measured/Predicted offsets (Fig. S6E)

LR04	"	"	"	"	"	"	"	"	"	"	10	0.48	0.27	-173	92	10	0.28	0.36	-41	82
LuntunedR04	"	"	"	"	"	"	"	"	"	"	10	0.36	0.32	-163	86	10	0.17	0.42	-25	75
HW04	"	"	"	"	"	"	"	"	"	"	10	0.16	0.43	-152	75	10	0.44	0.29	21	90
U1476pmag	"	"	"	"	"	"	"	"	"	"	10	0.26	0.37	-154	81	10	0.16	0.43	-40	74
All events	"	"	"	"	"	"	"	"	"	"	**40**	**0.01**	**0.35**	**-159**	**84**	**40**	**0.01**	**0.35**	**-25**	**83**
All events w/o LR04	"	"	"	"	"	"	"	"	"	"	**30**	**0.01**	**0.37**	**-156**	**80**	**30**	**0.03**	**0.35**	**-20**	**83**

3.2. Relative to local obliquity peak

3.2.1. Measured offsets

	Onset Deglac					Max Deglac					Peak IG					Max inception				
	n	p value	*r*	Angle	1σ	n	p value	*r*	Angle	1σ	n	p value	*r*	Angle	1σ	n	p value	*r*	Angle	1σ
LR04	10	0.00	0.98	-74	10			1	0		10	0.00	0.84	90	34	10	0.00	0.73	157	45
LuntunedR04	10	0.00	0.98	-73	10			1	0		10	0.00	0.80	89	38	10	0.01	0.69	144	50
HW04	10	0.00	0.99	-67	7			1	0		10	0.01	0.65	79	53	10	0.19	0.41	123	77
U1476pmag	10	0.00	0.95	-87	19			1	0		10	0.00	0.75	87	43	10	0.01	0.63	126	55
All events	**40**	**0.00**	**0.97**	**-75**	**14**			**1**	**0**		**40**	**0.00**	**0.76**	**87**	**43**	**40**	**0.00**	**0.60**	**140**	**58**
All events	**30**	**0.00**	**0.96**	**-75**	**15**			**1**	**0**		**30**	**0.00**	**0.73**	**85**	**45**	**30**	**0.00**	**0.57**	**133**	**61**

3.2.2. Measured/Predicted offsets (Fig. S6F)

LR04	"	"	"	"	"			"	"		10	0.00	0.83	98	35	10	0.00	0.74	156	44
LuntunedR04	"	"	"	"	"			"	"		10	0.00	0.78	97	40	10	0.01	0.65	157	54
HW04	"	"	"	"	"			"	"		10	0.02	0.63	91	55	10	0.25	0.37	157	80
U1476pmag	"	"	"	"	"			"	"		10	0.00	0.73	97	45	10	0.02	0.61	147	57
All events	"	"	"	"	"			"	"		**40**	**0.00**	**0.74**	**96**	**44**	**40**	**0.00**	**0.59**	**154**	**59**
All events	"	"	"	"	"			"	"		**30**	**0.00**	**0.71**	**95**	**47**	**30**	**0.00**	**0.54**	**153**	**64**

p > 0.1
p > 0.05

p > 0.1 wrt measured
r > 0.8 & *r* > 0.1 wrt measured

Table S2. Results for Scenarios I-III for individual benthic $\delta^{18}O$ records and combinations with and without LR04. Scenario I: All points are obtained directly from records on their original

timescales. Scenario II: Max deglac is set to the nearest precession peak. Scenario III: Max deglac is set to the nearest obliquity peak. In Scenarios II and III, measured offsets (relative to Max deglac) are obtained from the original records; predicted offsets are obtained from the relationships shown in Figures 2, S3, S4. Colour-coding is same as used in Figure S6